A&A 598, A135 (2017)
DOI: 10.1051/0004-6361/201629869

Astronomy & Astrophysics

Complete spectral energy distribution of the hot, helium-rich white dwarf RX J0503.9−2854⋆,⋆⋆,⋆⋆⋆,⋆⋆⋆⋆

D. Hoyer[1], T. Rauch[1], K. Werner[1], J. W. Kruk[2], and P. Quinet[3,4]

[1] Institute for Astronomy and Astrophysics, Kepler Center for Astro and Particle Physics, Eberhard Karls University, Sand 1, 72076 Tübingen, Germany
e-mail: rauch@astro.uni-tuebingen.de
[2] NASA Goddard Space Flight Center, Greenbelt, MD 20771, USA
[3] Physique Atomique et Astrophysique, Université de Mons – UMONS, 7000 Mons, Belgium
[4] IPNAS, Université de Liège, Sart Tilman, 4000 Liège, Belgium

Received 10 October 2016 / Accepted 17 October 2016

ABSTRACT

Context. In the line-of-sight toward the DO-type white dwarf RX J0503.9−2854, the density of the interstellar medium (ISM) is very low, and thus the contamination of the stellar spectrum almost negligible. This allows us to identify many metal lines in a wide wavelength range from the extreme ultraviolet to the near infrared.
Aims. In previous spectral analyses, many metal lines in the ultraviolet spectrum of RX J0503.9−2854 have been identified. A complete line list of observed and identified lines is presented here.
Methods. We compared synthetic spectra that had been calculated from model atmospheres in non-local thermodynamical equilibrium, with observations.
Results. In total, we identified 1272 lines (279 of them were newly assigned) in the wavelength range from the extreme ultraviolet to the near infrared. 287 lines remain unidentified. A close inspection of the EUV shows that still no good fit to the observed shape of the stellar continuum flux can be achieved although He, C, N, O, Al, Si, P, S, Ca, Sc, Ti, V, Cr, Mn, Fe, Cr, Ni Zn, Ga, Ge, As, Kr, Zr, Mo, Sn, Xe, and Ba are included in the stellar atmosphere models.
Conclusions. There are two possible reasons for the deviation between observed and synthetic flux in the EUV. Opacities from hitherto unconsidered elements in the model-atmosphere calculation may be missing, and/or the effective temperature is slightly lower than previously determined.

Key words. atomic data – line: identification – stars: abundances – stars: individual: RX J0503.9-2854 – virtual observatory tools

1. Introduction

The white dwarf (WD) RX J0503.9−2854 (henceforth RE 0503−289, WD 0501−289 McCook & Sion 1999a,b) was discovered in the ROSAT (ROentgen SATellite) wide field camera all-sky survey of extreme-ultraviolet (EUV) sources (Pounds et al. 1993). Barstow et al. (1993) reported its discovery by the Extreme Ultraviolet Explorer (EUVE), and identified it with a peculiar He-rich DO-type WD, namely MCT 0501−2858 in the Montreal-Cambridge-Tololo survey of southern hemisphere blue stars (Demers et al. 1986). They found that RE 0503−289 is located in a direction with very low density of the interstellar medium (ISM). In the line-of-sight (LOS) toward RE 0503−289, Vennes et al. (1994) measured a column density of $\log(N_{\rm H\,I}\,/\,{\rm cm}^{-2}) = 17.75-18.00$ using EUVE photometry data. Rauch et al. (2016a) resolved at least two ISM components in the LOS toward RE 0503−289 based on high-resolution and high signal-to-noise ultraviolet (UV) spectroscopy performed by Far Ultraviolet Spectroscopic Explorer (FUSE) and *Hubble* Space Telescope/Space Telescope Imaging Spectrograph (HST/STIS) and measured a very low ($E_{B-V} = 0.015 \pm 0.002$) interstellar reddening.

The almost negligible contamination by ISM line absorption allows us to identify even weak lines of many species from so far He up to trans-iron elements as heavy as Ba (Table 2). For reliable abundance analyses of these elements, a precise $T_{\rm eff}$ and $\log g$ determination is a prerequisite to keep error propagation as small as possible. An initial constraint of $T_{\rm eff} = 60\,000-70\,000$ K was given by Vennes et al. (1994) from EUV photometry. The first spectral analysis by means of non-local thermodynamic equilibrium (NLTE) stellar atmosphere models considering opacities of H, He, and C was published by Barstow et al. (1994). They found $T_{\rm eff} = 60\,000-80\,000$ K and $\log(g/{\rm cm/s}^2) = 7.5-8.0$. Dreizler & Werner (1996) used ultraviolet (UV) spectra in addition and NLTE model atmospheres and determined $T_{\rm eff} = 70\,000 \pm 5000$ K and $\log g = 7.5 \pm 0.5$. Recently, Rauch et al. (2016a) analyzed optical and ultraviolet

⋆ Based on observations with the NASA/ESA *Hubble* Space Telescope, obtained at the Space Telescope Science Institute, which is operated by the Association of Universities for Research in Astronomy, Inc., under NASA contract NAS5-26666.
⋆⋆ Based on observations made with the NASA-CNES-CSA Far Ultraviolet Spectroscopic Explorer.
⋆⋆⋆ Based on observations made with ESO Telescopes at the La Silla Paranal Observatory under program IDs 072.D-0362, 165.H-0588, and 167.D-0407.
⋆⋆⋆⋆ Tables A.1–A.5 are only available at the CDS via anonymous ftp to cdsarc.u-strasbg.fr (130.79.128.5) or via http://cdsarc.u-strasbg.fr/viz-bin/qcat?J/A+A/598/A135

Table 1. History of $T_{\rm eff}$ and $\log g$ determinations (cf., Müller-Ringat 2013).

$T_{\rm eff}$/kK	$\log g$	Model atmosphere	Method	Comment	Reference
60–90			EUV, PM	very low $N_{\rm H\,I}$	Barstow et al. (1993)
60–80			EUV, OPT	very low $N_{\rm H\,I}$	Barstow et al. (1993)
60–80	7.5–8.0	He, HHeC	NLTE, OPT, UV, EUV	EUV problem[a]	Barstow et al. (1994)
60–70			EUV, PM	very low $N_{\rm H\,I}$	Vennes et al. (1994)
70[b]	7.0	HeCNOSiFeNi	LTE, EUV, UV		Polomski et al. (1995)
65[c]	7.5[d]	HHeC	NLTE, OPT	no H detectable, upper limit 5% (mass fraction)	Werner (1996)
70	7.5	HHeCNOSi	NLTE, OPT, UV	$M = 0.49\,M_\odot$	Dreizler & Werner (1996)
66.6–70.4	7.13–7.27	HHe	LTE, UV	$M = 0.40\,M_\odot$	Vennes et al. (1998)
70[e]	7.5[e]		NLTE, diffusion	no good fit achieved	Dreizler (1999)
69–75	7.26–7.63	HHeC HHeCNOSiFeNi	NLTE, OPT, UV, EUV	EUV problem[a]	Barstow et al. (2000)
65–70	7.5[e]	HeCNi, HeONi	NLTE, EUV	EUV problem[a]	Werner et al. (2001)
70[e]	7.5[e]	HHeCNOSiFeNi+ PS	NLTE, UV LTE	EUV problem[a]	Barstow et al. (2007)
68–72	7.4–7.6	HeCNOAlSiPS+ CaScTiVCrMnFeCrNi+ ZnGaGeAsKrZrMoSnXeBa	NLTE, OPT, UV	$M = 0.514^{+0.15}_{-0.05}\,M_\odot$	Rauch et al. (2016a)

Notes. PM denotes photometry. [(a)] Section 7, [(b)] adopted upper limit of Vennes et al. (1994), [(c)] adopted value close to lower limit of Barstow et al. (1994), [(d)] adopted from Barstow et al. (1994), [(e)] adopted from Dreizler & Werner (1996).

(FUSE and HST/STIS) spectra and significantly reduced the error limits to ±2000 K and ±0.1, respectively. Table 1 summarizes previous analyses.

2. Observations

In this paper, we used the observed spectra that are briefly described in the following. If they are compared to synthetic spectra, the latter are convolved with Gaussians to model the respective instrument's resolution.

Extreme ultraviolet: observations by the EUVE observatory were performed using the short-wavelength (70 Å $< \lambda <$ 190 Å), the medium-wavelength (140 Å $< \lambda <$ 380 Å), and the long-wavelength (280 Å $< \lambda <$ 760 Å) spectrometers with a resolving power of $R \approx 300$. Details of the data reduction are given by Dupuis et al. (1995).

Far ultraviolet: spectra (910 Å $< \lambda <$ 1190 Å, $R \approx 20\,000$) were obtained with FUSE. Their data IDs are M1123601 (2000-12-04), M1124201 (2001-02-02), and P2041601 (2000-12-05). The spectra were shifted to rest wavelengths and co-added. For details see Werner et al. (2012b).

Ultraviolet: spectroscopy was performed with HST/STIS on 2014-08-14. Two observations with grating E140M (1144 Å $< \lambda <$ 1709 Å, $R \approx 45\,800$) and two observations with grating E230M (1690 Å $< \lambda <$ 2366 Å, 2277 Å $< \lambda <$ 3073 Å, $R \approx 30\,000$) were co-added. These observations are retrievable from the Barbara A. Mikulski Archive for Space Telescopes (MAST).

Optical: spectra (3290 Å $< \lambda <$ 4524 Å, 4604 Å $< \lambda <$ 5609 Å, 5673 Å $< \lambda <$ 6641 Å) were obtained on 2000-09-09 and 2001-04-08 in the framework of the Supernova Ia Progenitor Survey project (SPY, Napiwotzki et al. 2001, 2003). The Ultraviolet and Visual Echelle Spectrograph (UVES) attached to the Very Large Telescope (VLT) located at the European Southern Observatory (ESO) on Cerro Paranal in Chile was employed to achieve a resolution of about 0.2 Å. In addition, we use a spectrum taken with the Echelle Multi Mode Instrument (EMMI) attached to the New Technology Telescope (NTT; 1992-01, 4094 Å $< \lambda <$ 4994 Å, resolution of about 3.0 Å).

Near infrared: spectroscopy (9500 Å $< \lambda <$ 13 420 Å, $R \approx 950$) was performed on 2003-12-10 using the Son-of-Isaac (SofI) instrument at the NTT. The spectrum used here was digitized with Dexter[1] from Fig. 1 in Dobbie et al. (2005).

3. Model atmospheres and atomic data

The stellar model atmospheres used for this paper were calculated with our Tübingen NLTE Model Atmosphere Package (TMAP[2], Werner et al. 2003, 2012a). They assume plane-parallel geometry, are chemically homogeneous, and in hydrostatic and radiative equilibrium. An adaptation is the New Generation Radiative Transport (NGRT) code (Dreizler & Wolff 1999; Schuh et al. 2002) that can consider diffusion in addition to calculate stratified stellar atmospheres.

The Tübingen Model Atom Database (TMAD[3]) provides ready-to-use model atoms in TMAP format for many species up to Ba. TMAD has been constructed as part of the Tübingen contribution to the German Astrophysical Virtual Observatory (GAVO[4]).

Werner et al. (2012b) discovered lines of trans-iron elements, namely Ga (atomic number $Z = 31$), Ge (32), As (33), Se (34), Kr (36), Mo (42), Sn (50), Te (52), I (53), and Xe (54), in the FUSE spectrum of RE 0503−289. For precise abundance determinations of these species, reliable atomic data is mandatory. For example, reliable transition probabilities are required, not only for lines that are identified in the observation but for the complete model atoms that are considered in the model-atmosphere calculations. Due to the lack of such data, Werner et al. (2012b) were restricted to abundance determinations of Kr and Xe only.

[1] http://dc.zah.uni-heidelberg.de/sdexter
[2] http://astro.uni-tuebingen.de/~TMAP
[3] http://astro.uni-tuebingen.de/~TMAD
[4] http://www.g-vo.org

Table 2. Photospheric abundances (mass fraction) of RE 0503−289.

Element	Abundance	1st Line identifications
He	9.73×10^{-1}	Barstow et al. (1994)
C	2.22×10^{-2}	Barstow et al. (1994)
N	5.49×10^{-5}	Dreizler & Werner (1996)
O	2.94×10^{-3}	Polomski et al. (1995), Dreizler & Werner (1996)
Al	5.01×10^{-5}	Rauch et al. (2016a)
Si	1.60×10^{-4}	Polomski et al. (1995), Dreizler & Werner (1996)
P	1.06×10^{-6}	Vennes et al. (1998), Barstow et al. (2007)
S	3.96×10^{-5}	Barstow et al. (2007)
Ni	7.25×10^{-5}	Barstow et al. (2000)
Zn	1.13×10^{-4}	Rauch et al. (2014a)
Ga	3.44×10^{-5}	Werner et al. (2012b), Rauch et al. (2015b)
Ge	1.58×10^{-4}	Werner et al. (2012b), Rauch et al. (2012)
As	1.60×10^{-5}	Werner et al. (2012b)
Se		Werner et al. (2012b)
Kr	5.04×10^{-4}	Werner et al. (2012b), Rauch et al. (2016a)
Zr	3.00×10^{-4}	Rauch et al. (2016a)
Mo	1.88×10^{-4}	Rauch et al. (2016b)
Sn	2.06×10^{-4}	Werner et al. (2012b)
Te		Werner et al. (2012b)
I		Werner et al. (2012b)
Xe	1.26×10^{-4}	Werner et al. (2012b), Rauch et al. (2015a), Rauch et al. (2016a)
Ba	3.57×10^{-4}	Rauch et al. (2014b)

Notes. The reference for the 1st line identifications is given in the final column.

Table 3. Newly calculated transition probabilities.

Element	Ions	Reference
Zn	IV–V	Rauch et al. (2014a)
Ga	IV–VI	Rauch et al. (2015b)
Ge	V–VI	Rauch et al. (2012)
Kr	IV–VII	Rauch et al. (2016a)
Zr	IV–VII	Rauch et al. (2016a)
Tc	II– VI	Werner et al. (2015)
Mo	IV–VII	Rauch et al. (2016b)
Xe	IV–VII	Rauch et al. (2015a, 2016a)
Ba	V–VII	Rauch et al. (2014b)

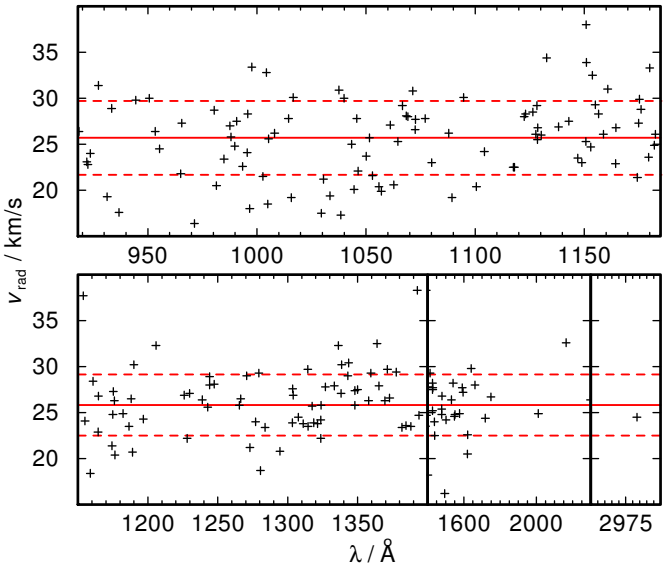

Fig. 1. Determination of v_{rad} from individual lines in the FUSE (*top panel*) and HST/STIS observations (*bottom*). The full horizontal lines indicate the average v_{rad} for FUSE and HST/STIS, respectively. The dashed lines show the 1σ error.

We initiated the calculation of new transition probabilities that were then used to determine the abundance of the respective element. Table 3 gives an overview of the so far calculated data. To provide easy access to this data, the registered Tübingen Oscillator Strengths Service (TOSS) has been created within the GAVO project.

To construct model atoms for the use within TMAP, the elements given in Table 3 require the calculation of so-called super levels and super lines with our Iron Opacity and Interface (IrOnIc, Rauch & Deetjen 2003) due to the very high number of atomic levels and lines. We transferred the TOSS data into Kurucz's data format[5] that can be read by IrOnIc.

4. Radial velocity and gravitational redshift

To shift the observation to rest wavelength, we determined the radial velocity v_{rad} of RE 0503−289 from FUSE and HST/STIS spectra. To measure the wavelengths of the line centers, we used IRAF[6] to fit Gaussians to the line profiles. In total, we evaluated 100 lines in the FUSE wavelength range and 103 lines in the STIS wavelength range (Fig. 1). The averages are $v_{rad}^{FUSE} = 25.7 \pm 4.2$ km s^{-1} and $v_{rad}^{STIS} = 25.8 \pm 3.7$ km s^{-1}. We adopted the mean value of $v_{rad} = 25.7^{+3.6}_{-4.0}$ km s^{-1}. From this value, the gravitational redshift z has to be subtracted. To calculate z and the respective radial velocity, we created the GAVO tool Tübingen Gravitational REDshift calculator (TGRED, Fig. C.2). For RE 0503−289, we derive $v_{rad}^{gred} = 15.5^{+6.7}_{-4.6}$ km s^{-1}. The true radial velocity is then $v_{rad}^{RE\,0503-289} = 10.2^{+8.2}_{-8.6}$ km s^{-1}.

5. Line identification

To unambiguously identify lines in our observed spectra (Sect. 2), we used the best synthetic model of Rauch et al. (2016a) and calculated additional spectra with oscillator strengths set to zero for individual elements. This allows to find weak lines, even if they are blended by stronger lines. The detection limit is an equivalent width of $W_\lambda = 2$ mÅ. Table 4 shows the total numbers of lines identified in the four wavelength ranges and the numbers of lines that were suited to determine W_λ and v_{rad}. The current line lists are presented in Tables A.1–A.5, a regularly updated version is available online[7].

[5] http://kurucz.harvard.edu/atoms.html

[6] IRAF is distributed by the National Optical Astronomy Observatory, which is operated by the Associated Universities for Research in Astronomy, Inc., under cooperative agreement with the National Science Foundation.

[7] http://astro.uni-tuebingen.de/~hoyer/objects/RE0503-289

Table 4. Statistics of the identified (in brackets: newly identified in this paper) and unidentified lines in the observed spectra.

Wavelength	Numbers of lines			W_λ	$v_{\rm rad}$
range	total	identified	unidentified		
EUV	74	74(35)	0	0	0
FUV	616	536(55)	76	148	100
NUV	790	579(120)	211	252	103
optical	83	83(69)	0	0	0
NIR	2	2(0)	0	0	0

Notes. The last two columns give the numbers of lines that were used to measure their equivalent widths W_λ and $v_{\rm rad}$ (Fig. 1), respectively.

6. Visualization and online line list

In the framework of the Tübingen GAVO project, we have developed the registered Tübingen VISisualization tool (TVIS) that allows the user to plot any data in an easy way on the WWW. The plotter itself is written in HTML5 and Javascript. To strongly increase the security of this web application, no Flash or Java is necessary to use it, meaning that TVIS will even work when Flash is dead and Java applets are blocked by the browsers.

The comparison of our best model spectra with the available observation of RE 0503−289 in the EUV, FUV, NUV, and optical wavelength ranges was realized with TVIS and is shown online[8]. Figures B.1 to B.3 show the FUV to optical range.

7. Is there still an EUV problem in RE 0503–289?

To analyze the EUVE observation, Barstow et al. (1995) used NLTE model atmospheres that were calculated with the code that is nowadays called TMAP. A synthetic spectrum (scaled to match the observed EUV flux) that was calculated from a model with $T_{\rm eff} = 70\,000$ K, $\log g = 7.0$, C/He = 1%, and N/He = 0.01% (the latter being number ratios) reproduced well the observation. A major problem arose, however, from the fact that the model flux (reddened and interstellar neutral hydrogen absorption considered) in the wavelength range 228 Å $< \lambda <$ 400 Å was about an order of magnitude higher than observed. Only models with $T_{\rm eff} < 65\,000$ K produced an acceptable fit. He I λ 5875.62 Å ($2p\,^3P^o$–$3d\,^3D$) in the optical wavelength range (e.g., in spectra taken with the TWIN spectrograph at the Calar Alto observatory and in SPY spectra, Dreizler & Werner 1996; Rauch et al. 2016a) establishes a stringent constraint of $T_{\rm eff} = 70\,000 \pm 2000$ K.

Werner et al. (2001) calculated TMAP models that were composed of He, C, O, and the iron-group elements (Ca–Ni). Interstellar He I absorption was applied in addition to that of H I. The flux discrepancy was reduced (model flux three times higher than observed) but the basic problem, finding an agreement at $T_{\rm eff} = 70\,000$ K, was not solved.

Müller-Ringat (2013) created the Tübingen EUV absorption tool (TEUV, Fig. C.1), that corrects synthetic stellar fluxes for ISM absorption for $\lambda < 911$ Å. Presently, only radiative bound-free absorption of the lowest ionization states of H, He, C, N, and O is simulated. Opacity Project data (Seaton et al. 1994) is used for the photoionization cross-sections. These consider, for example, autoionization features. For this paper, Si has been added to TEUV. Two interstellar components with different radial and turbulent velocities, temperatures, and column densities can be considered. Müller-Ringat (2013) calculated TMAP models ($T_{\rm eff} = 70\,000$ K, $\log g = 7.5$) that included He, C, N, O, and the iron-group elements. Although Kurucz's line lists were strongly extended in 2009 (Kurucz 2009, 2011), and about a factor of ten more iron-group lines were considered, the EUV model flux was about twice as high as that observed. To match the observed EUV flux, $T_{\rm eff}$ had to be reduced to $\lesssim$65 000 K.

Rauch et al. (2016a) determined $T_{\rm eff} = 70\,000 \pm 2000$ K and $\log g = 7.5 \pm 0.1$ in a detailed reanalysis of optical and UV spectra. They included 27 elements, namely He, C, N, O, Al, Si, P, S, Ca, Sc, Ti, V, Cr, Mn, Fe, Cr, Ni, Zn, Ga, Ge, As, Kr, Zr, Mo, Sn, Xe, and Ba, in their models. From these, we calculated the EUV spectrum (228 Å $\leq \lambda \leq$ 910 Å) with 1601 atomic levels treated in NLTE, considering 2481 lines of the elements He–S and about 30 million lines of the elements with $Z \geq 20$. The frequency grid comprised 174 873 points with $\Delta\lambda \leq 0.005$ Å.

Figure 2 demonstrates the determination of the interstellar reddening. We apply the reddening data of Morrison & McCammon (1983, provided for 1.26 Å $\leq \lambda \leq$ 413 Å and extrapolated toward the He I ground-state threshold) and Fitzpatrick (1999, $\lambda \geq 911$ Å). Between the He I ground-state edge and the H I Lyman edge, only absorption due to H I is considered. To determine E_{B-V}, we normalized our models to the 2MASS H brightness (14.766 ± 0.063, Cutri et al. 2003a,b). To match the observed flux level between about 400 Å to 600 Å, $E_{B-V} = 0.00026 \pm 0.00003$ is necessary. This is less than $E_{B-V} = 0.015 \pm 0.002$ that was used by Rauch et al. (2016a) to

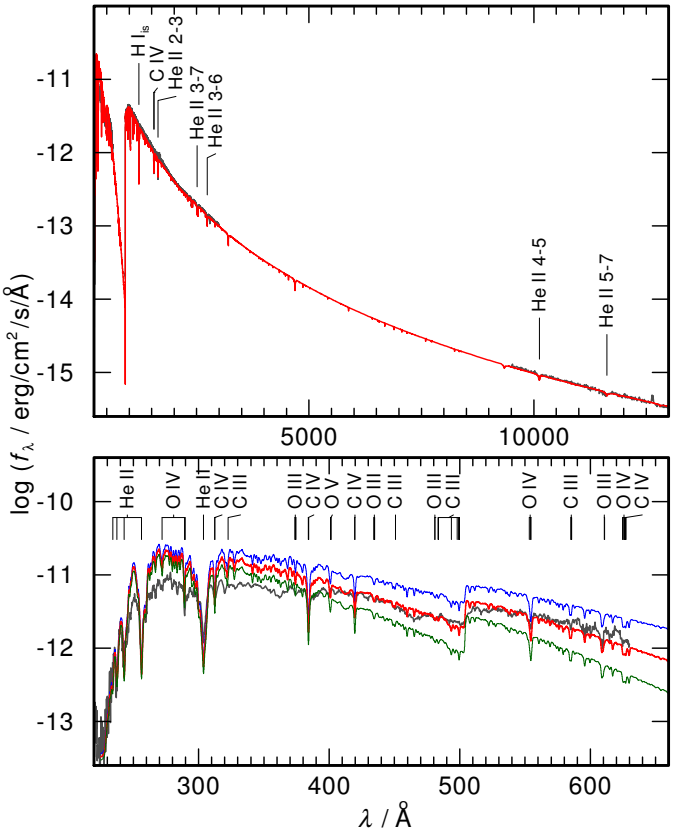

Fig. 2. Determination of E_{B-V}. *Top*: reddening with $E_{B-V} = 0.00026$ applied to our synthetic spectrum in the wavelength range from the EUV to the NIR. *Bottom*: same like top panel, for $E_{B-V} = 0.00016$ (blue), 0.00026 (red), and 0.00036 (green) in the EUV wavelength range. Prominent lines are marked.

[8] http://astro.uni-tuebingen.de/~TVIS/objects/RE0503-289

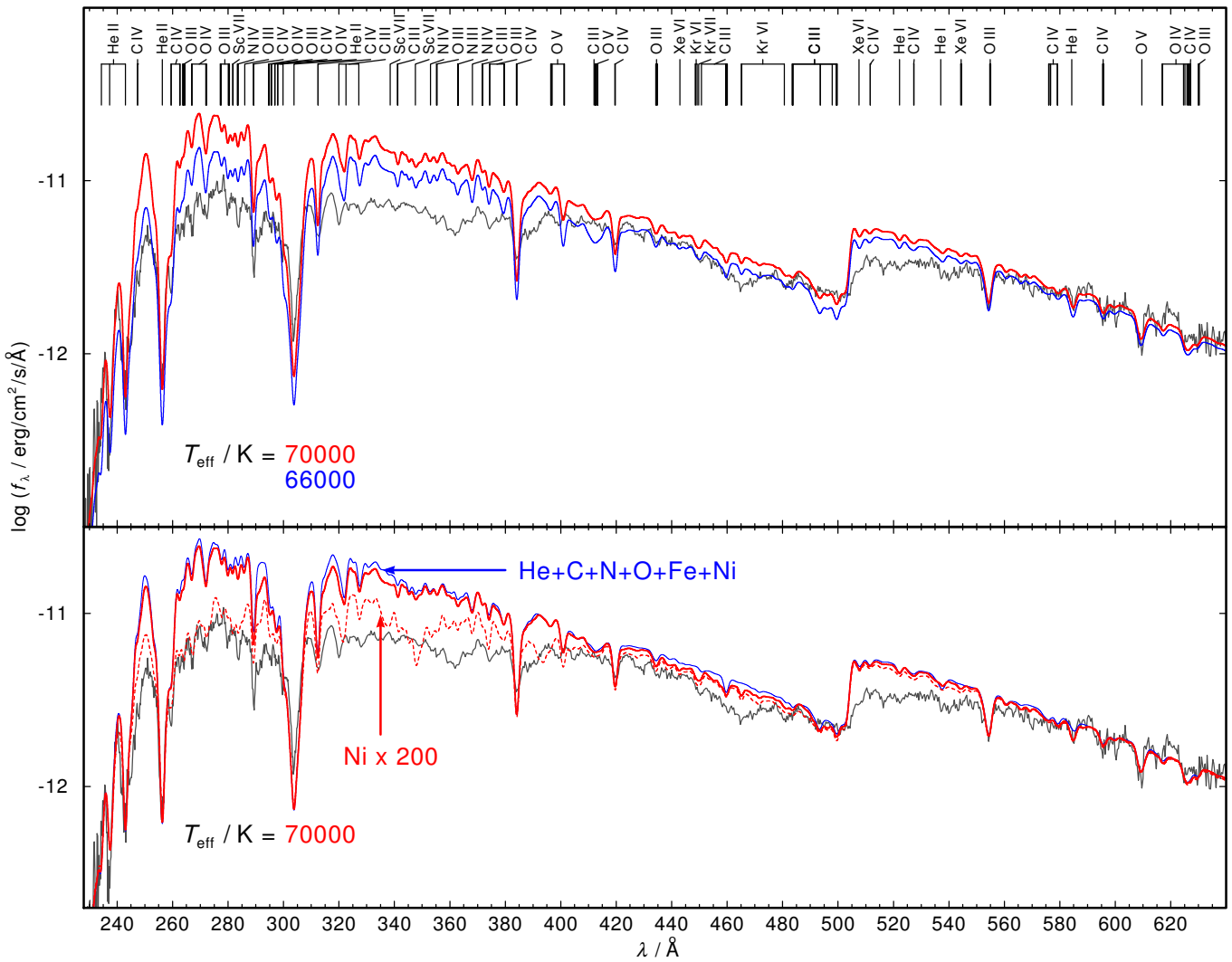

Fig. 3. Comparison of the EUVE observation (gray line in both panels) with our models. *Top panel*: two models with $T_{\rm eff} = 70\,000$ K (red) and $T_{\rm eff} = 66\,000$ K (blue). Identified photospheric lines are marked at the top. *Bottom panel*: three models with $T_{\rm eff} = 70\,000$ K. Red, thick line: model from the top panel, red, dashed line: model with 200 times increased Ni abundance, blue, thin line: model that considered only opacities of He, C, N, O, Fe, and Ni.

reproduce the observed FUSE flux level. With the Galactic reddening law of Groenewegen & Lamers (1989, $\log(N_{\rm H\,I}/E_{B-V} = 21.58 \pm 0.1$) and the total cloud column density of interstellar H I of $1.5 \pm 0.2 \times 10^{18}$ cm^{-2} (measured from Lβ, Rauch et al. 2016a), we can calculate $E_{B-V} = 0.00039^{+0.00017}_{-0.00012}$ which is within error limits well in agreement with our result.

A close look at the EUV wavelength range shows still a significant difference between model and observation (Fig. 3, top panel), most prominent between 250 Å and 400 Å and between 504 Å and 550 Å. Our present models reduced the deviation by about a factor of two compared the models of Werner et al. (2001). The EUV problem cannot be solved by using a cooler model, even at $T_{\rm eff} = 66\,000$ K, which is already outside the error range of $T_{\rm eff} = 70\,000 \pm 2000$ K given by Rauch et al. (2016a), no sufficient improvement is achieved. The impact of metal opacities is demonstrated in Fig. 3 by a model that considered only opacities from He, C, N, O, Fe, and Ni with same abundance ratios like our best model. To test the impact of additional opacity, we artificially increased the Ni abundance by factor of 200 to match the model's flux to the observed between 250 Å and 280 Å. This reduced the flux discrepancy between 300 Å and 400 Å as well while the wavelength region above the He I ground-state threshold is unaffected. However, we conclude that even in our advanced models opacity is missing from elements that are hitherto not considered. To include, for example, other trans-iron elements requires detailed laboratory measurements of their spectra and the extensive calculation of transition probabilities.

8. What is the nature of RE 0503–289?

RE 0503−289 was first classified to be a DO-type WD (Barstow et al. 1993). Its optical spectrum exhibits an absorption trough around C IV $\lambda\lambda$ 4646.62−4687.95 Å and He II λ 4685.80 Å. This trough is the spectroscopic criterion for the H-deficient PG 1159-type stars (e.g., Werner & Herwig 2006). Figure 4 shows the comparison of the wavelength region around this trough for the PG 1159 prototype PG 1159−035 (V⋆ GW Vir, WD 1159−035, $T_{\rm eff} = 140\,000 \pm 5000$ K, $\log g = 7.0 \pm 0.5$, Jahn et al. 2007) and the O(He)-type WD KPD 0005+5106 (WD 0005+511, $T_{\rm eff} = 195\,000 \pm 15\,000$ K, $\log g = 6.7 \pm 0.2$, Werner & Rauch 2015). Both objects are at an earlier state of stellar evolution

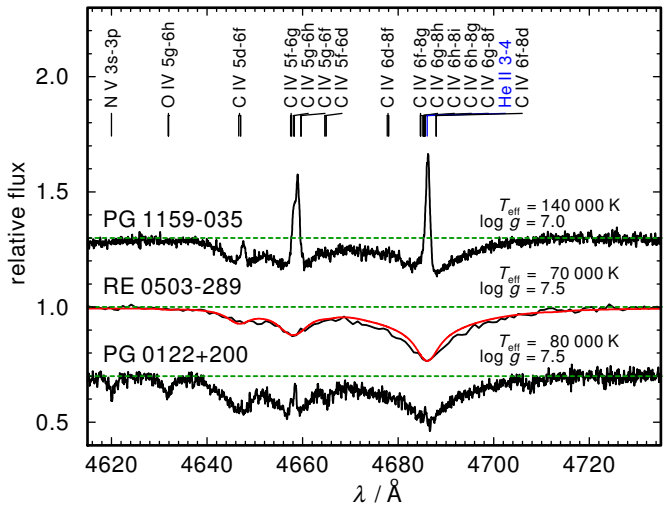

Fig. 4. Section of the optical spectra of PG 1159−035 (from SPY, shifted by 0.3 in flux units), RE 0503−289 (EMMI), and PG 0122+200 (Keck, shifted by −0.3; *from top to bottom*) around the PG 1159 absorption trough. For RE 0503−289, the synthetic spectrum of Rauch et al. (2016a) is overplotted (red line). The green, dashed lines indicate the continuum level.

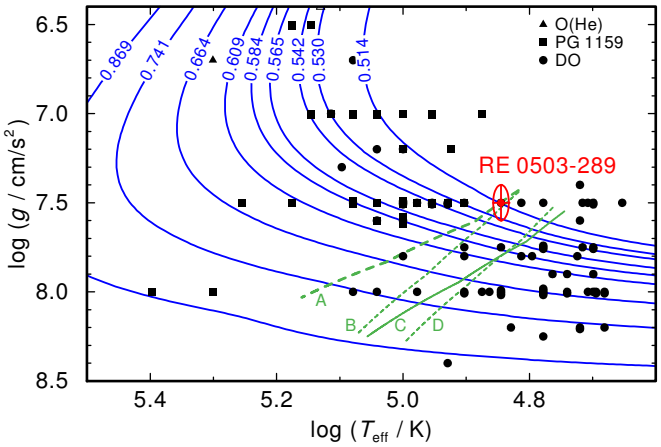

Fig. 5. Location of RE 0503−289 and related objects (Hügelmeyer et al. 2006; Kepler et al. 2016; Reindl et al. 2014b,a; Werner & Herwig 2006) in the log $T_{\rm eff}$–log g plane (cf., http://www.star.le.ac.uk/~nr152/He.html for stellar parameters). Evolutionary tracks for H-deficient WDs (Althaus et al. 2009) labeled with their respective masses in $M_{\odot}$ are plotted for comparison. Transition limits predicted by Unglaub & Bues (2000) are indicated (see text for details).

than RE 0503−289. The strengths of the PG 1159 absorption troughs are almost the same for the much hotter PG 1159−035 and RE 0503−289, although their photospheric C abundances are significantly different, ≈48% by mass (Jahn et al. 2007) and ≈2%, respectively. The cool PG 1159-type star PG 0122+200 has about 22% of C in its photosphere (Werner & Rauch 2014).

In a log $T_{\rm eff}$–log g diagram (Fig. 5), RE 0503−289 is located at the so-called PG 1159 wind limit (Unglaub & Bues 2000, their Fig. 13, digitized with Dexter) that was predicted for a ten-times-reduced mass-loss rate (line A, calculated with $\dot{M} = 1.29 \times 10^{-15} L^{1.86}$ from Bloecker 1995; Pauldrach et al. 1988). This line approximately separates the regions that are populated by PG 1159-type stars and DO-type WDs. Lines B and C in Fig. 5 show where the photospheric C content is reduced by factors of 0.5 and 0.1, respectively, when using the mass-loss rate given above. To the right of line D, no PG 1159 star is located.

Werner et al. (2014) suggested a mass ratio C/He = 0.02 to conserve previously assigned spectroscopic classes. However, PG 1159 stars span a wide range of C/He (0.03−0.33, Werner et al. 2014).

RE 0503−289 is located close to line B of Unglaub & Bues (2000) in Fig. 5, that is, its C abundance should be already reduced by a factor of 0.5. Thus, it is likely that RE 0503−289 had a C/He ≈ 0.05 in its antecedent PG 1159-star phase. Even now, its C/He lies a bit higher than 0.02 and RE 0503−289 may be classified as a PG 1159 star as well. This is corroborated by the still high efficiency of radiative levitation that is responsible for the extremely high overabundances of trans-iron elements (Rauch et al. 2016b). However, the transition from a PG 1159-type star to a DO-type star is smooth and RE 0503−289 is an ideal object to study this in detail. Unfortunately, the strong radiative levitation of trans-iron elements wipes out all information about their asymptotic giant branch (AGB) abundances and RE 0503−289 is not suited to constrain AGB nucleosynthesis models.

9. Results

RE 0503−289 fulfills criteria of PG 1159 star and of DO-type WD classifications. The presence of the strong PG 1159 absorption trough around He II λ 4685.80 Å (Fig. 4) shows that RE 0503−289 could be classified as a PG 1159 star, although its C abundance would then be the lowest of this group. It is located close to the so-called PG 1159 wind limit (Fig. 5), meaning that it is close to the regime in which gravitation will dominate and pull metals down, out of the atmosphere. The strongly increased abundances of trans-iron elements, however, indicate that radiative levitation is still efficiently counteracting this process. Thus, RE 0503−289 has not arrived in its final stage of evolution. Formally, due to its log g > 7, the DO-type WD classification is right.

In the observed spectra, we identified 1272 lines in the wavelength range from the extreme ultraviolet to the near infrared. 287 lines remain unidentified. The best model of Rauch et al. (2016a) reproduces well most of the identified lines.

The EUV problem (Sect. 7) – the difference between observed and synthetic flux in the EUV is still present. Our advanced model atmospheres include opacities of 27 metals but their flux in the EUV is still partly about a factor of approximately two too high compared with the observation. We expect that missing metal opacities are the reason for this discrepancy.

Acknowledgements. D.H. and T.R. are supported by the German Aerospace Center (DLR, grants 50 OR 1501 and 05 OR 1507, respectively). The German Astrophysical Virtual Observatory (GAVO) project at Tübingen had been supported by the Federal Ministry of Education and Research (BMBF, 05 AC 6 VTB, 05 AC 11 VTB). Financial support from the Belgian FRS-FNRS is also acknowledged. P.Q. is research director of this organization. Some of the data presented in this paper were obtained from the Mikulski Archive for Space Telescopes (MAST). STScI is operated by the Association of Universities for Research in Astronomy, Inc., under NASA contract NAS5-26555. Support for MAST for non-HST data is provided by the NASA Office of Space Science via grant NNX09AF08G and by other grants and contracts. We thank Ralf Napiwotzki for putting the reduced ESO/VLT spectra at our disposal. The TEUV tool (http://astro-uni-tuebingen.de/~TEUV), the TGRED tool (http://astro-uni-tuebingen.de/~TGRED), the TIRO service (http://astro-uni-tuebingen.de/~TIRO), the TMAD service (http://astro-uni-tuebingen.de/~TMAD), the TOSS service (http://astro-uni-tuebingen.de/~TOSS), and the TVIS tool (http://astro-uni-tuebingen.de/~TVIS) used for this paper were constructed as

part of the activities of the German Astrophysical Virtual Observatory. This work used the profile-fitting procedure OWENS developed by M. Lemoine and the FUSE French Team. This research has made use of NASA's Astrophysics Data System and of the SIMBAD database operated at CDS, Strasbourg, France.

References

Althaus, L. G., Panei, J. A., Miller Bertolami, M. M., et al. 2009, ApJ, 704, 1605
Barstow, M. A., Wesemael, F., Holberg, J. B., et al. 1993, Adv. Space Res., 13, 281
Barstow, M. A., Holberg, J. B., Werner, K., Buckley, D. A. H., & Stobie, R. S. 1994, MNRAS, 267, 653
Barstow, M. A., Holberg, J. B., Koester, D., Nousek, J. A., & Werner, K. 1995, in White Dwarfs (Berlin: Springer Verlag), eds. D. Koester, & K. Werner, Lect. Notes Phys., 443, 302
Barstow, M. A., Dreizler, S., Holberg, J. B., et al. 2000, MNRAS, 314, 109
Barstow, M. A., Dobbie, P. D., Forbes, A. E., & Boyce, D. D. 2007, in 15th European Workshop on White Dwarfs, eds. R. Napiwotzki, & M. R. Burleigh, ASP Conf. Ser., 372, 243
Bloecker, T. 1995, A&A, 299, 755
Cutri, R. M., Skrutskie, M. F., van Dyk, S., et al. 2003a, 2MASS All Sky Catalog of point sources
Cutri, R. M., Skrutskie, M. F., van Dyk, S., et al. 2003b, VizieR Online Data Catalog: II/246
Demers, S., Beland, S., Kibblewhite, E. J., Irwin, M. J., & Nithakorn, D. S. 1986, AJ, 92, 878
Dobbie, P. D., Burleigh, M. R., Levan, A. J., et al. 2005, A&A, 439, 1159
Dreizler, S. 1999, A&A, 352, 632
Dreizler, S., & Werner, K. 1996, A&A, 314, 217
Dreizler, S., & Wolff, B. 1999, A&A, 348, 189
Dupuis, J., Vennes, S., Bowyer, S., Pradhan, A. K., & Thejll, P. 1995, ApJ, 455, 574
Fitzpatrick, E. L. 1999, PASP, 111, 63
Groenewegen, M. A. T., & Lamers, H. J. G. L. M. 1989, A&AS, 79, 359
Hügelmeyer, S. D., Dreizler, S., Homeier, D., et al. 2006, A&A, 454, 617
Jahn, D., Rauch, T., Reiff, E., et al. 2007, A&A, 462, 281
Kepler, S. O., Pelisoli, I., Koester, D., et al. 2016, MNRAS, 455, 3413
Kurucz, R. L. 2009, in AIP Conf. Ser. 1171, eds. I. Hubeny, J. M. Stone, K. MacGregor, & K. Werner, 43
Kurucz, R. L. 2011, Can. J. Phys., 89, 417
McCook, G. P., & Sion, E. M. 1999a, ApJS, 121, 1
McCook, G. P., & Sion, E. M. 1999b, VizieR Online Data Catalog: III/210
Morrison, R., & McCammon, D. 1983, ApJ, 270, 119
Müller-Ringat, E. 2013, Dissertation, University of Tübingen, Germany, http://nbn-resolving.de/urn:nbn:de:bsz:21-opus-67747
Napiwotzki, R., Christlieb, N., Drechsel, H., et al. 2001, Astron. Nachr., 322, 411
Napiwotzki, R., Christlieb, N., Drechsel, H., et al. 2003, The Messenger, 112, 25
Pauldrach, A., Puls, J., Kudritzki, R. P., Mendez, R. H., & Heap, S. R. 1988, A&A, 207, 123
Polomski, E. F., Vennes, S., & Chayer, P. 1995, in BAAS, AAS Meeting Abstracts, 27, 1311
Pounds, K. A., Allan, D. J., Barber, C., et al. 1993, MNRAS, 260, 77
Rauch, T., & Deetjen, J. L. 2003, in Stellar Atmosphere Modeling, eds. I. Hubeny, D. Mihalas, & K. Werner, ASP Conf. Ser., 288, 103
Rauch, T., Werner, K., Biémont, É., Quinet, P., & Kruk, J. W. 2012, A&A, 546, A55
Rauch, T., Werner, K., Quinet, P., & Kruk, J. W. 2014a, A&A, 564, A41
Rauch, T., Werner, K., Quinet, P., & Kruk, J. W. 2014b, A&A, 566, A10
Rauch, T., Hoyer, D., Quinet, P., Gallardo, M., & Raineri, M. 2015a, A&A, 577, A88
Rauch, T., Werner, K., Quinet, P., & Kruk, J. W. 2015b, A&A, 577, A6
Rauch, T., Gamrath, S., Quinet, P., et al. 2016a, A&A, 590, A128
Rauch, T., Quinet, P., Hoyer, D., et al. 2016b, A&A, 587, A39
Reindl, N., Rauch, T., Werner, K., et al. 2014a, A&A, 572, A117
Reindl, N., Rauch, T., Werner, K., Kruk, J. W., & Todt, H. 2014b, A&A, 566, A116
Schuh, S. L., Dreizler, S., & Wolff, B. 2002, A&A, 382, 164
Seaton, M. J., Yan, Y., Mihalas, D., & Pradhan, A. K. 1994, MNRAS, 266, 805
Unglaub, K., & Bues, I. 2000, A&A, 359, 1042
Vennes, S., Dupuis, J., Bowyer, S., et al. 1994, ApJ, 421, L35
Vennes, S., Dupuis, J., Chayer, P., et al. 1998, ApJ, 500, L41
Werner, K. 1996, A&A, 309, 861
Werner, K., & Herwig, F. 2006, PASP, 118, 183
Werner, K., & Rauch, T. 2014, A&A, 569, A99
Werner, K., & Rauch, T. 2015, A&A, 583, A131
Werner, K., Deetjen, J. L., Rauch, T., & Wolff, B. 2001, in 12th European Workshop on White Dwarfs, eds. J. L. Provencal, H. L. Shipman, J. MacDonald, & S. Goodchild, ASP Conf. Ser., 226, 55
Werner, K., Deetjen, J. L., Dreizler, S., et al. 2003, in Stellar Atmosphere Modeling, eds. I. Hubeny, D. Mihalas, & K. Werner, ASP Conf. Ser., 288, 31
Werner, K., Dreizler, S., & Rauch, T. 2012a, TMAP: Tübingen NLTE Model-Atmosphere Package, Astrophysics Source Code Library [record ascl:1212.015]
Werner, K., Rauch, T., Ringat, E., & Kruk, J. W. 2012b, ApJ, 753, L7
Werner, K., Rauch, T., & Kepler, S. O. 2014, A&A, 564, A53
Werner, K., Rauch, T., Kučas, S., & Kruk, J. W. 2015, A&A, 574, A29

Appendix A: Identified and unidentified lines in the spectrum of RE 0503–289

Tables A.1−A.5 are available at the CDS.

Appendix B: Observed spectra of RE 0503–289 compared with our best model

In the following figures, we show the comparison of our synthetic spectra with the FUSE (Fig. B.1, HST/STIS (Fig. B.2, and optical (Fig. B.3 observations. A visualization via TVIS is available at http://astro.uni-tuebingen.de/~TVIS/objects/RE0503-289

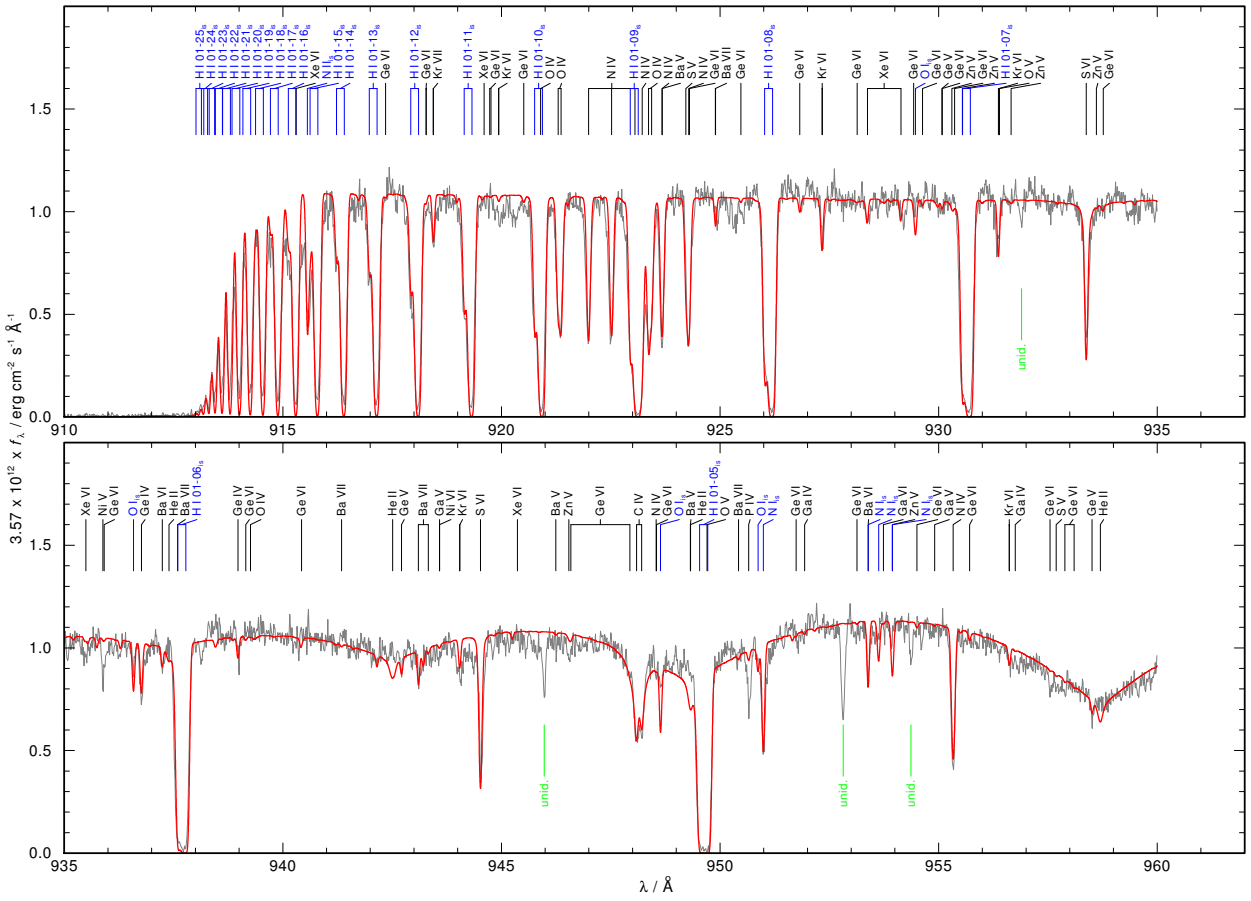

Fig. B.1. FUSE observation (gray) compared with the best model (red). Stellar lines are identified at top. "unid." denotes unidentified lines.

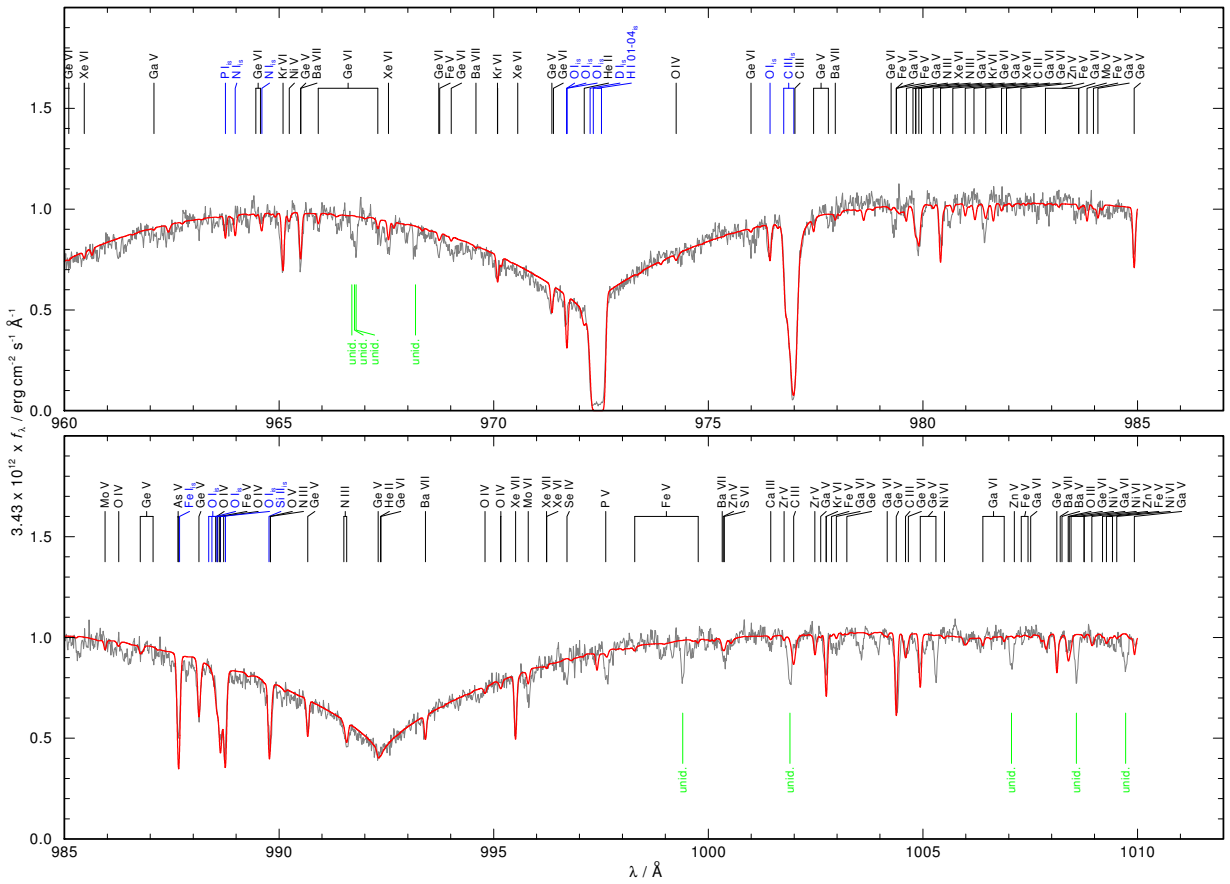

Fig. B.1. continued.

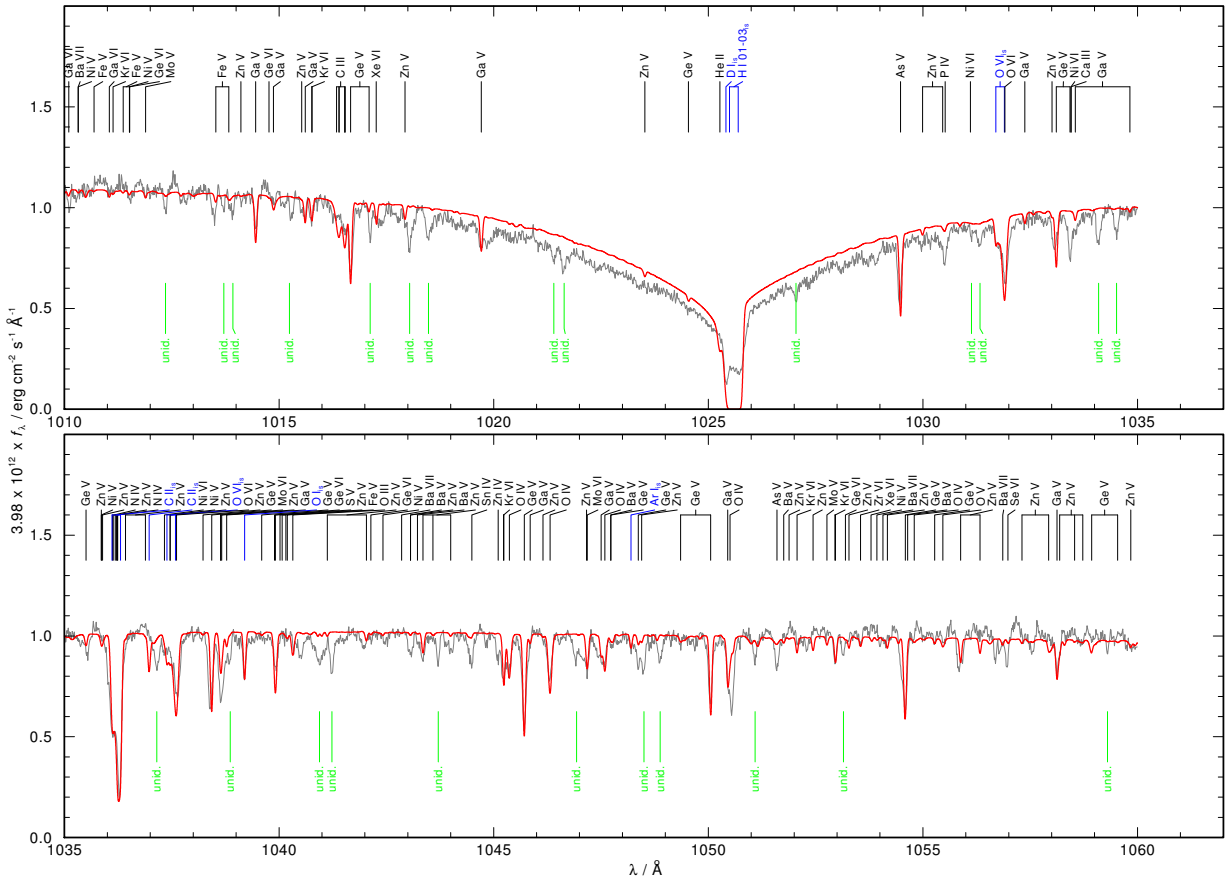

Fig. B.1. continued.

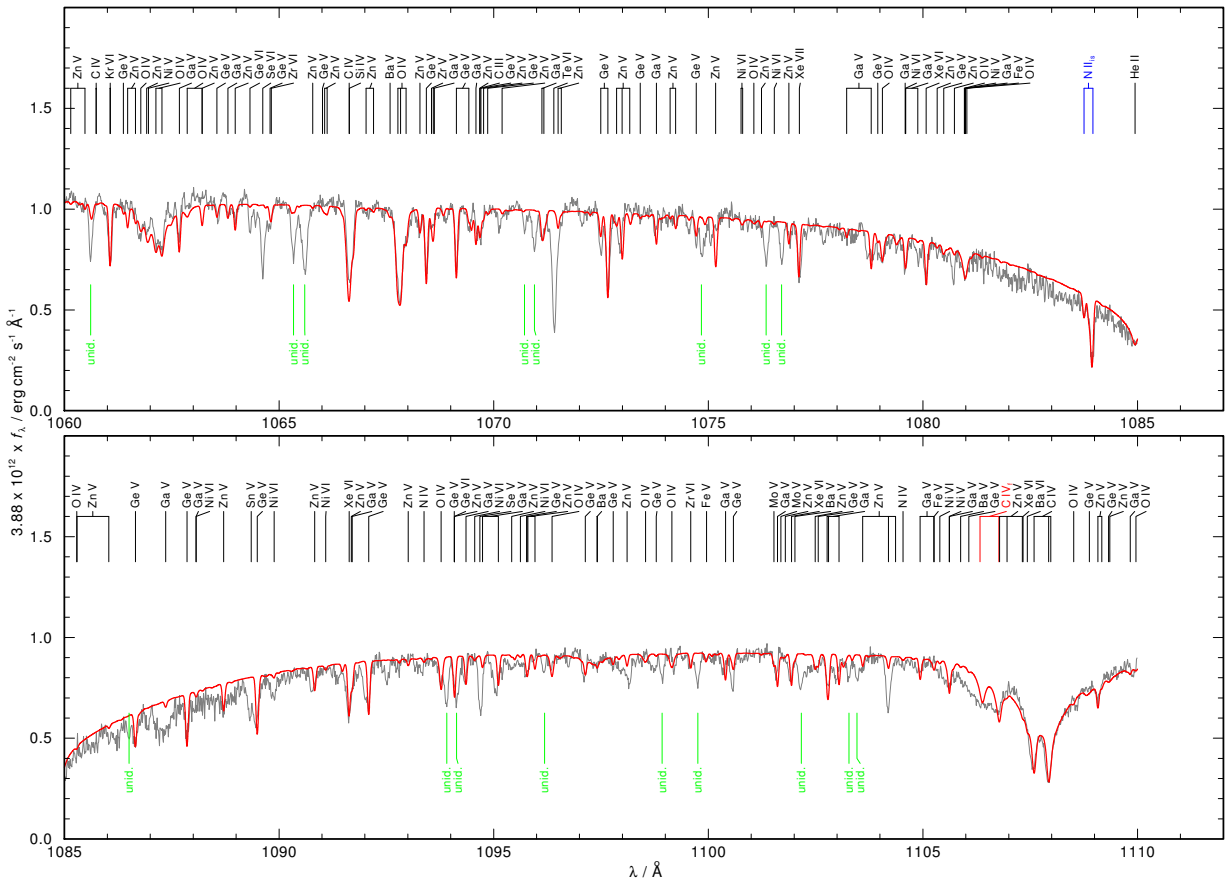

Fig. B.1. continued.

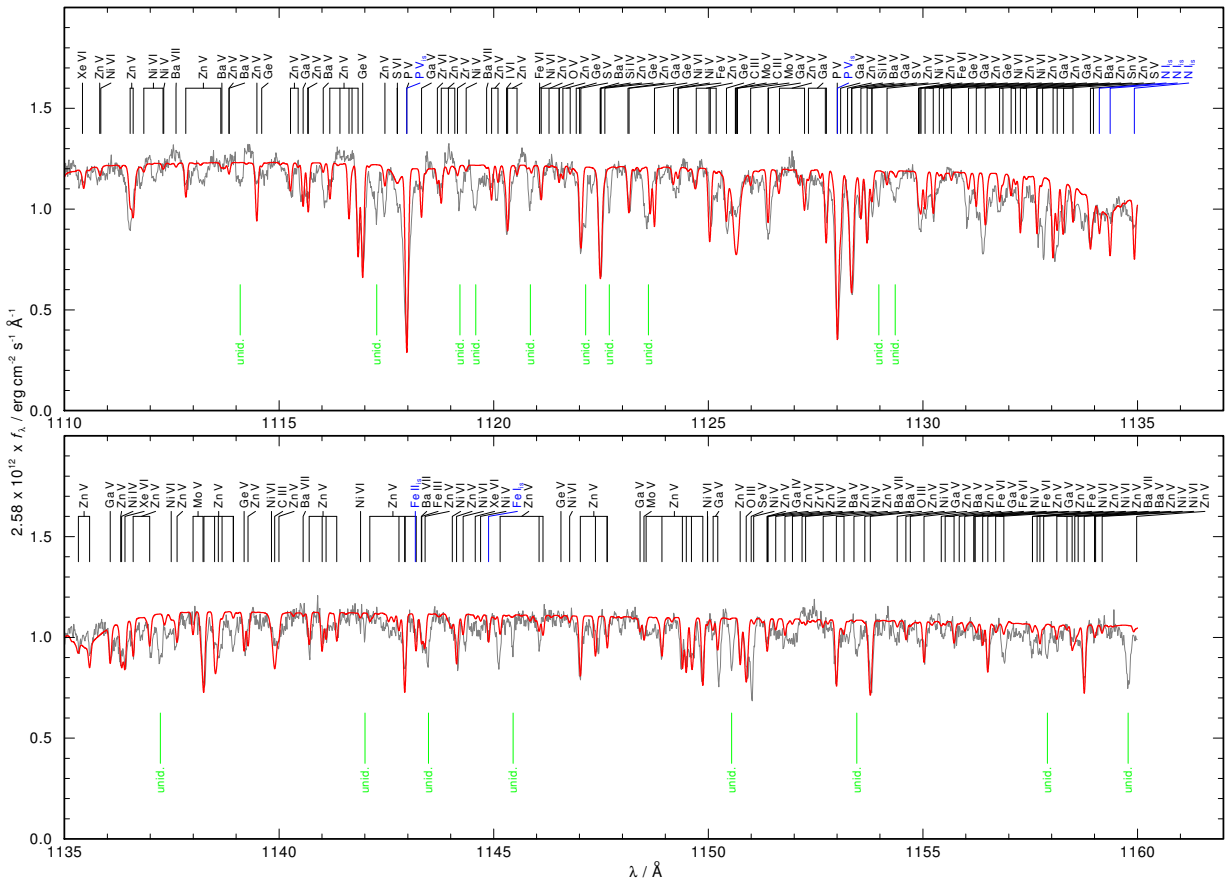

Fig. B.1. continued.

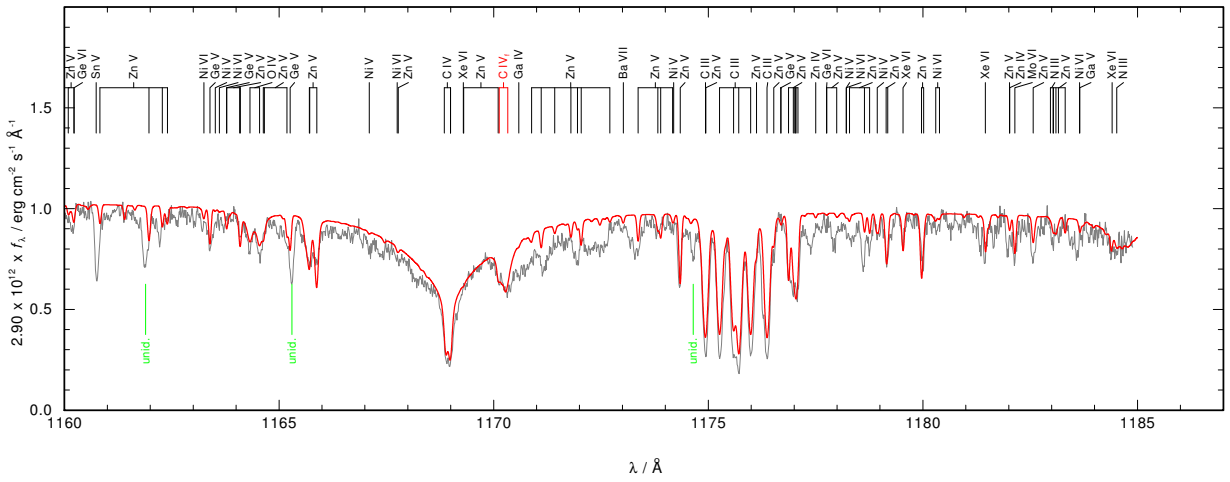

Fig. B.1. continued.

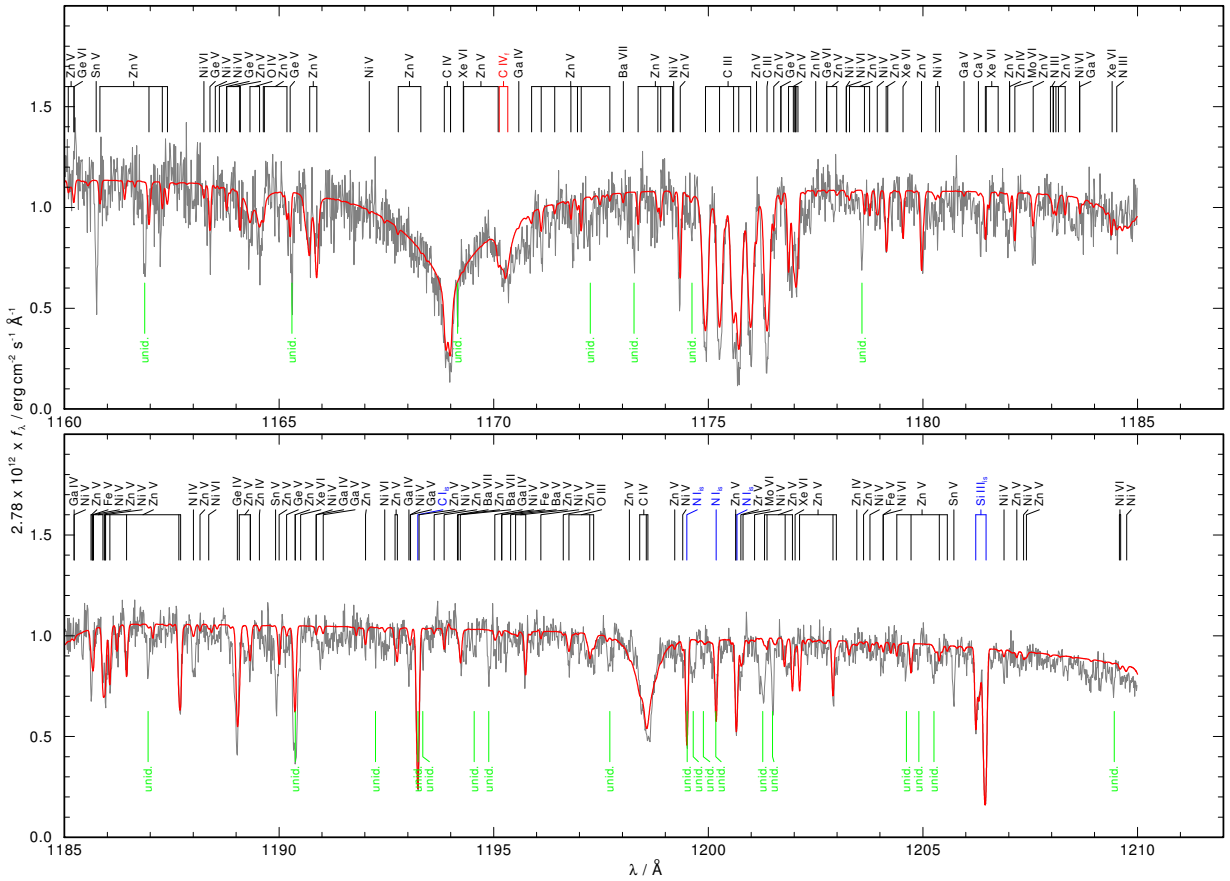

Fig. B.2. HST/STIS observation (gray) compared with the best model (red). Stellar lines are identified at top. “unid.” denotes unidentified lines.

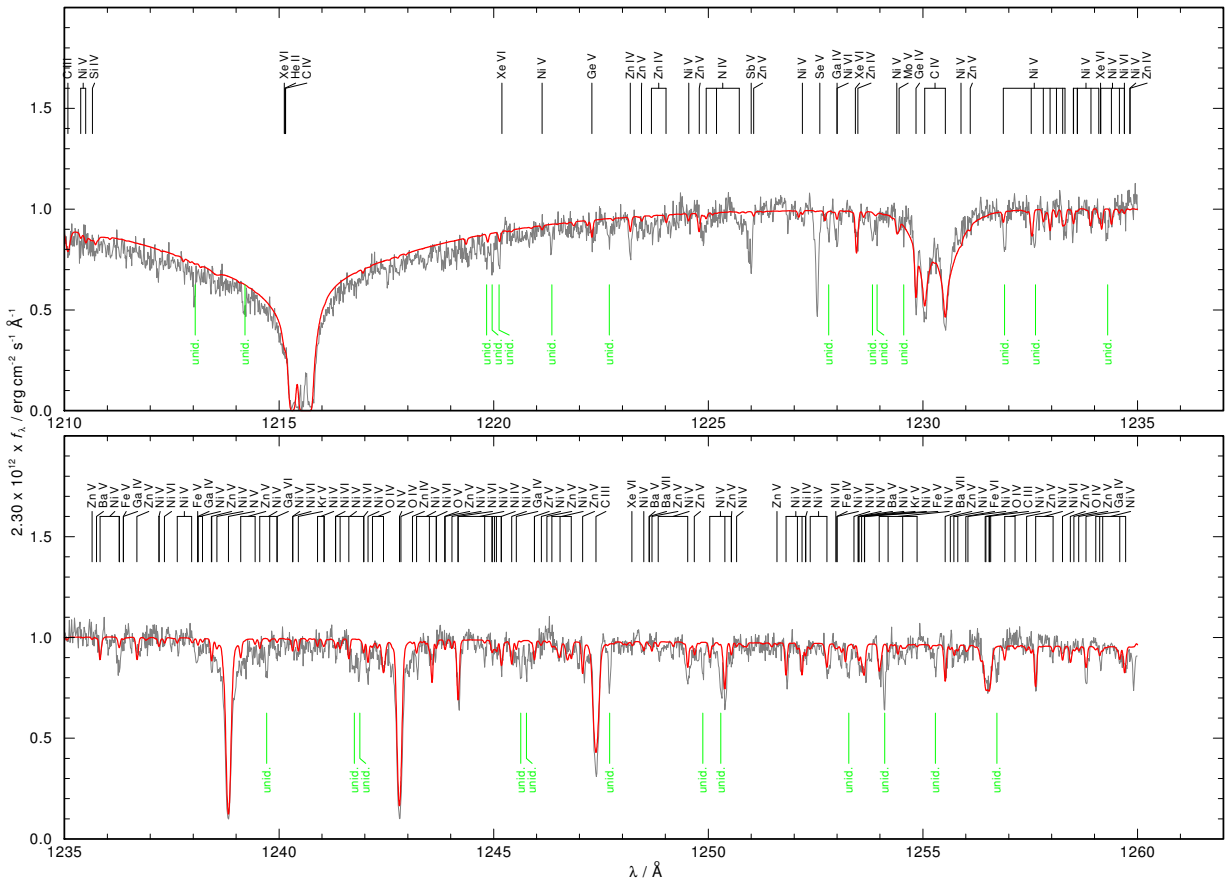

Fig. B.2. continued.

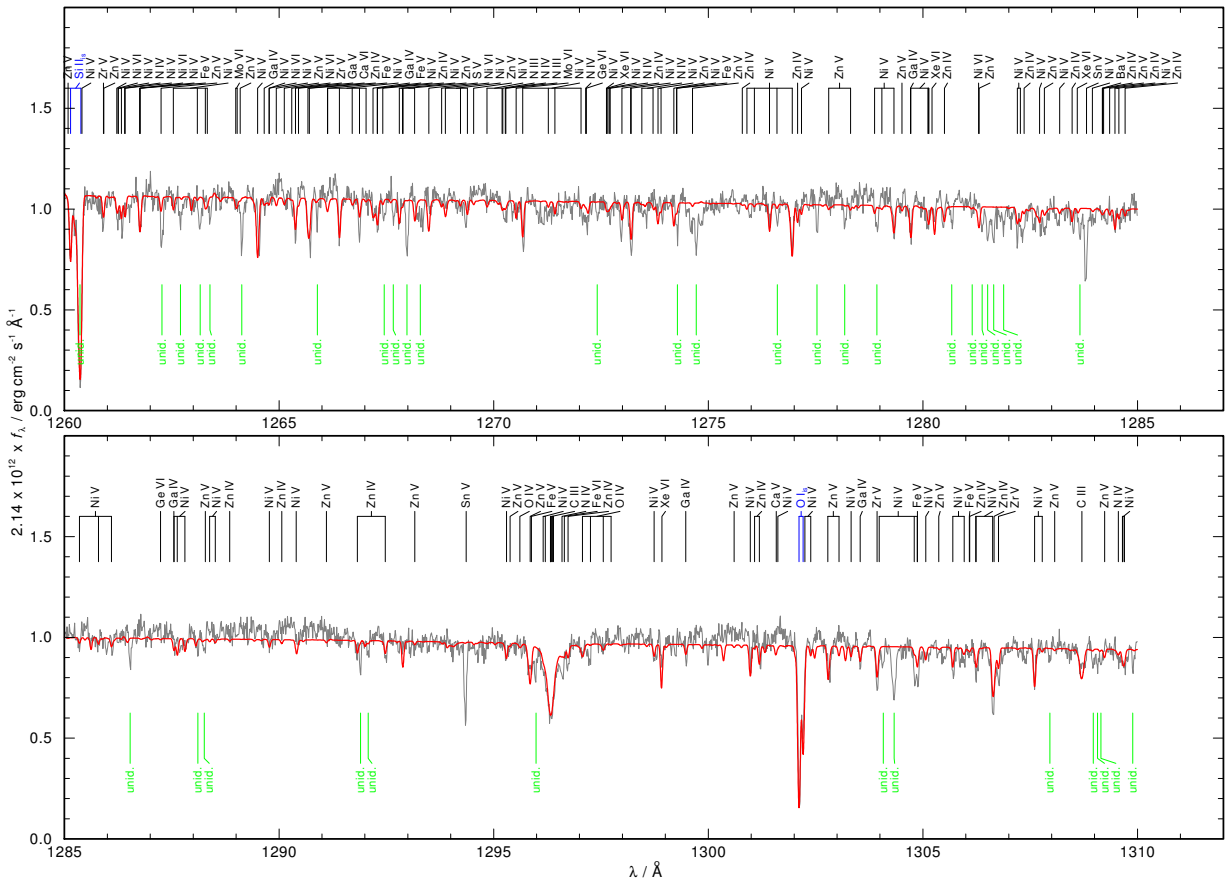

Fig. B.2. continued.

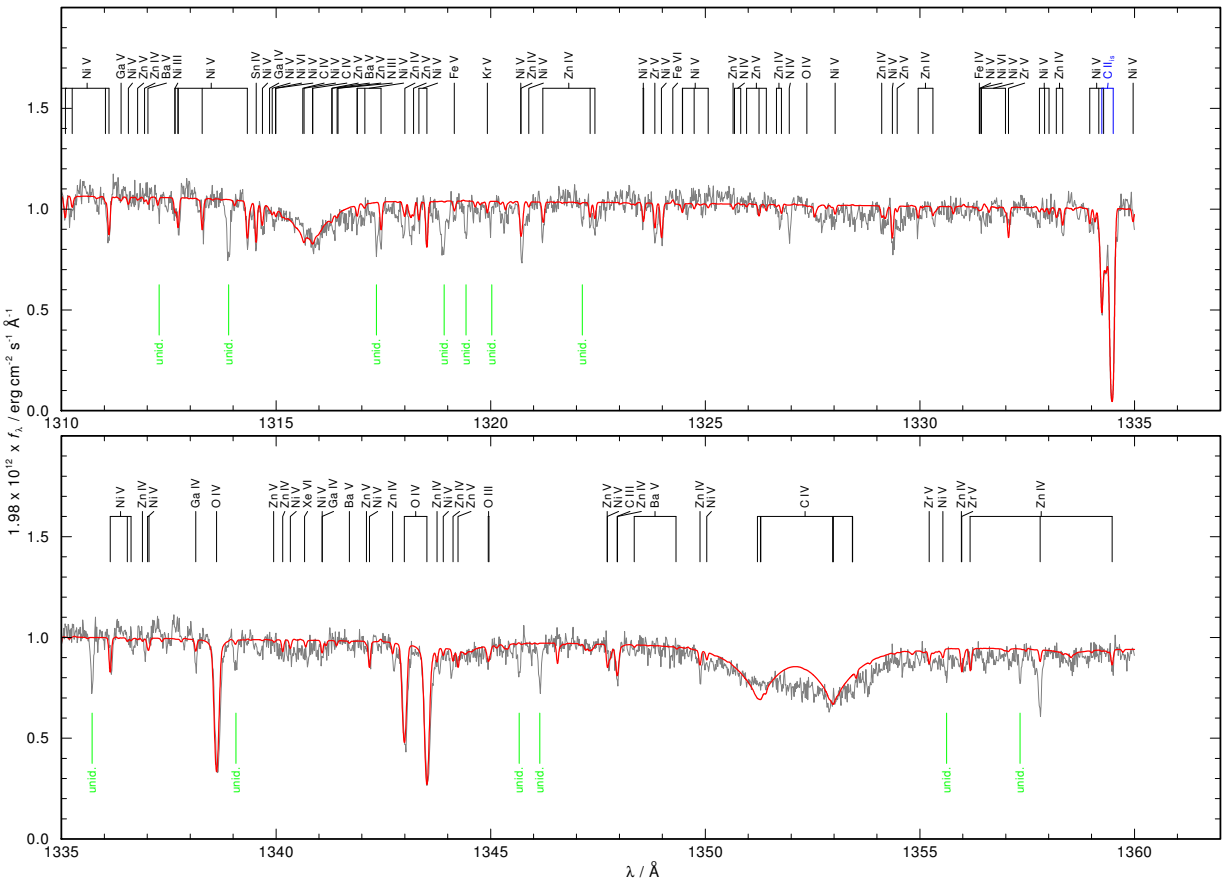

Fig. B.2. continued.

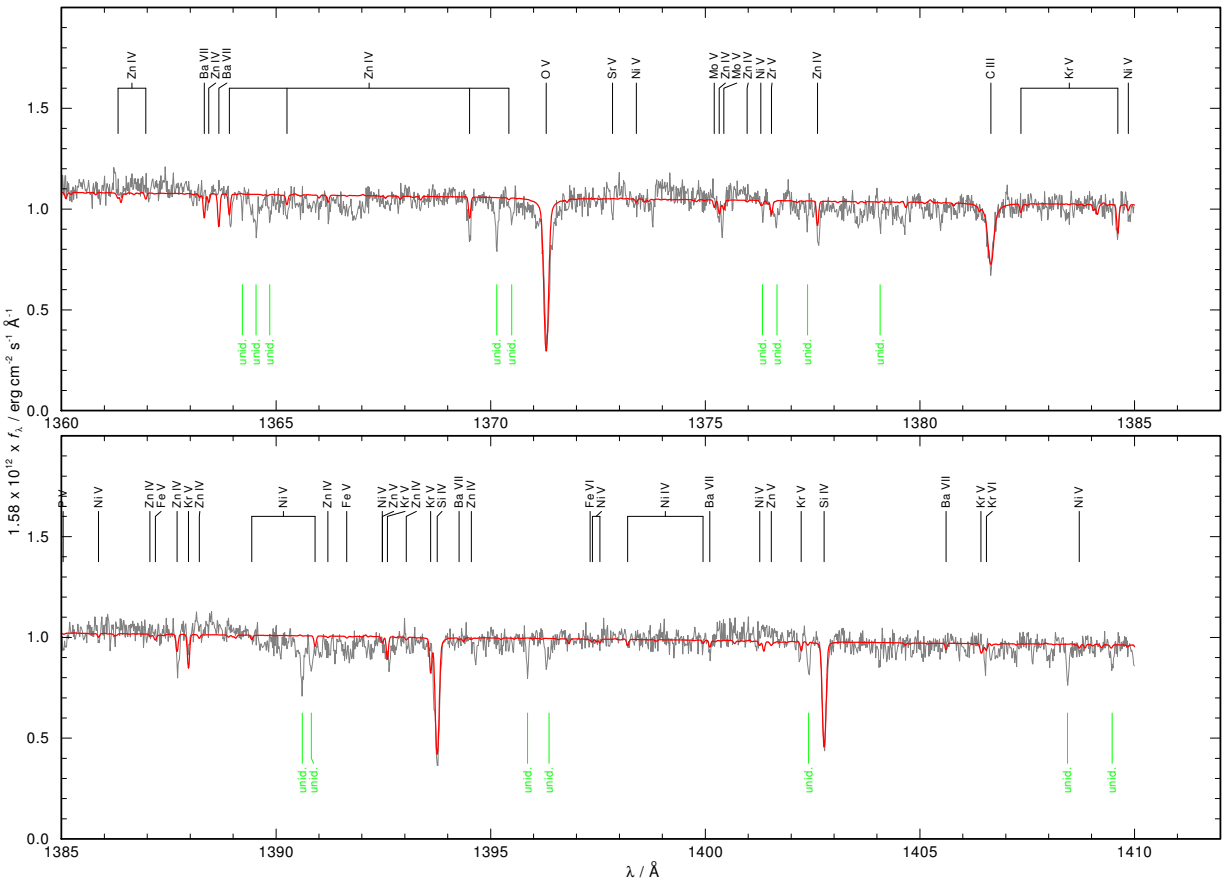

Fig. B.2. continued.

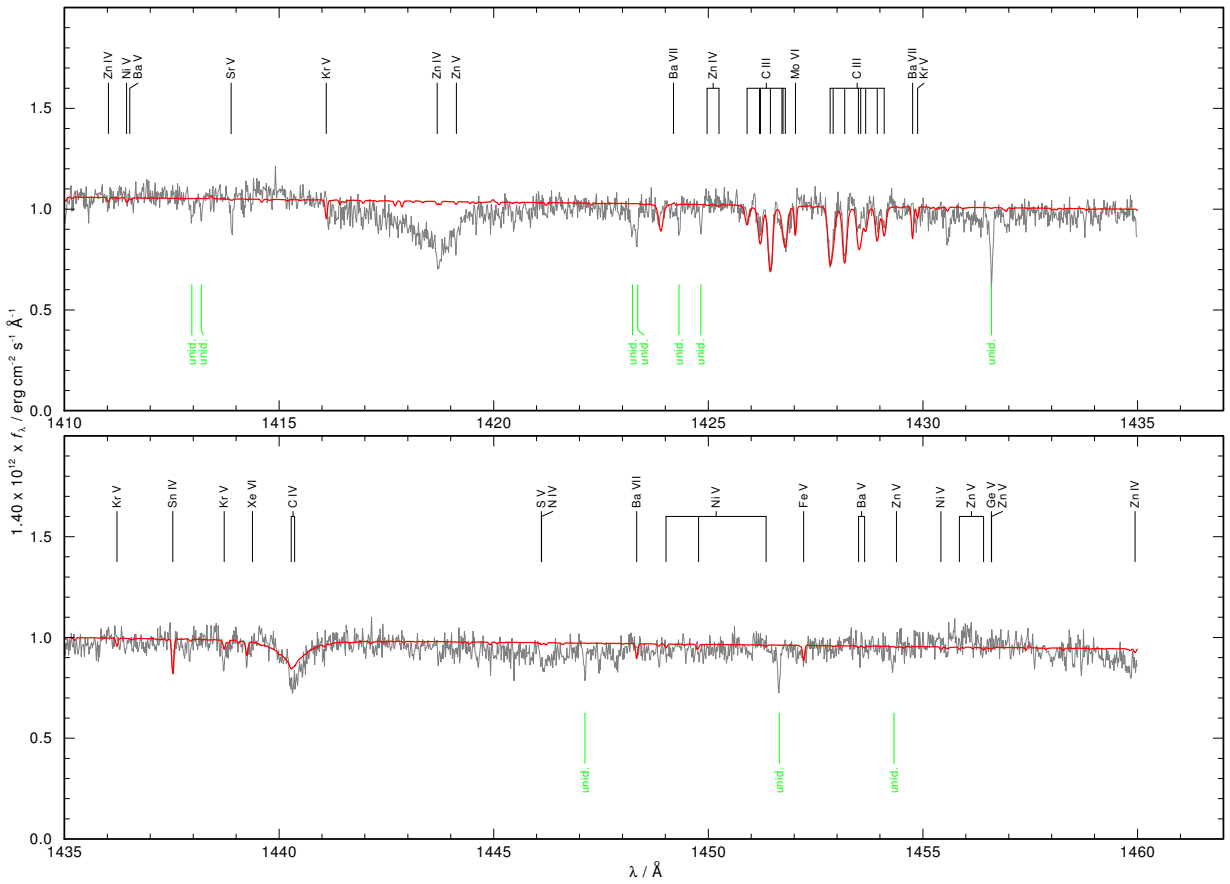

Fig. B.2. continued.

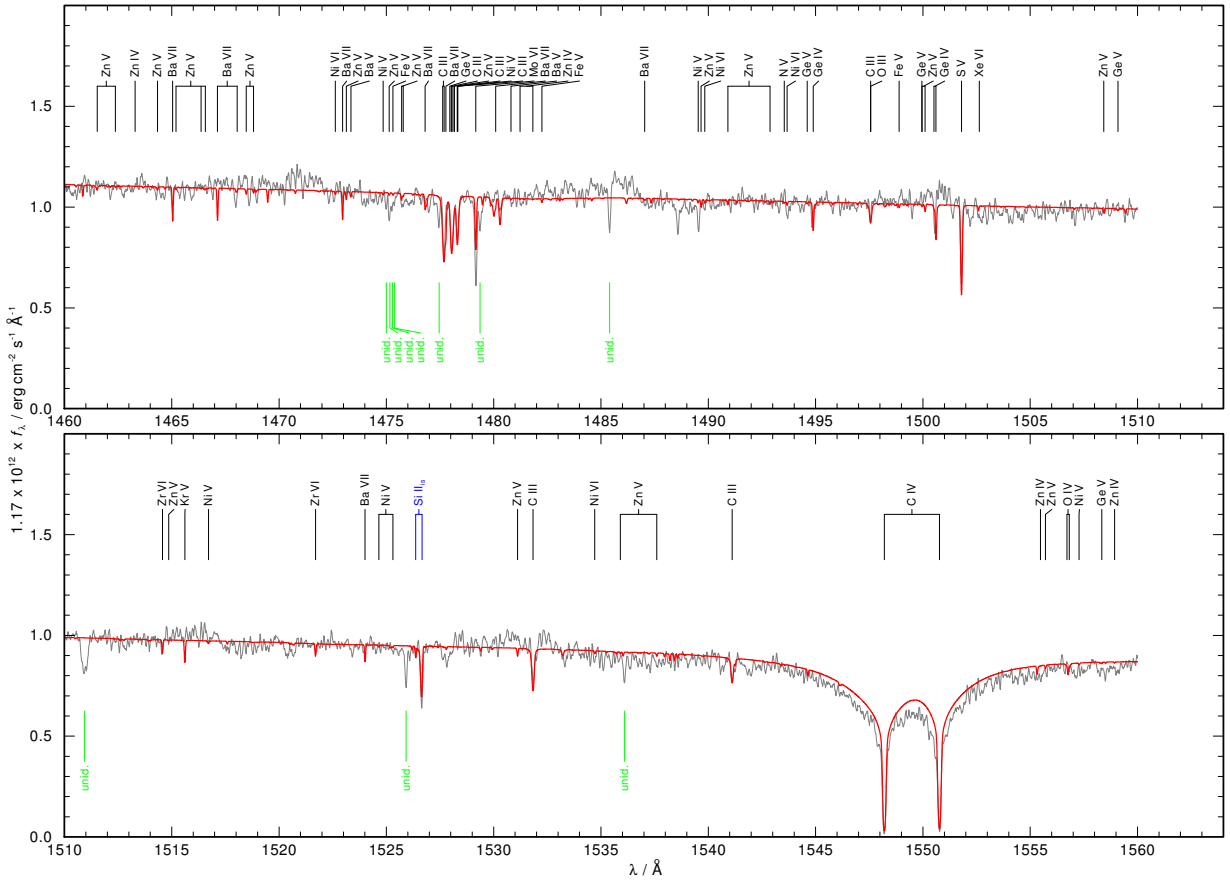

Fig. B.2. continued.

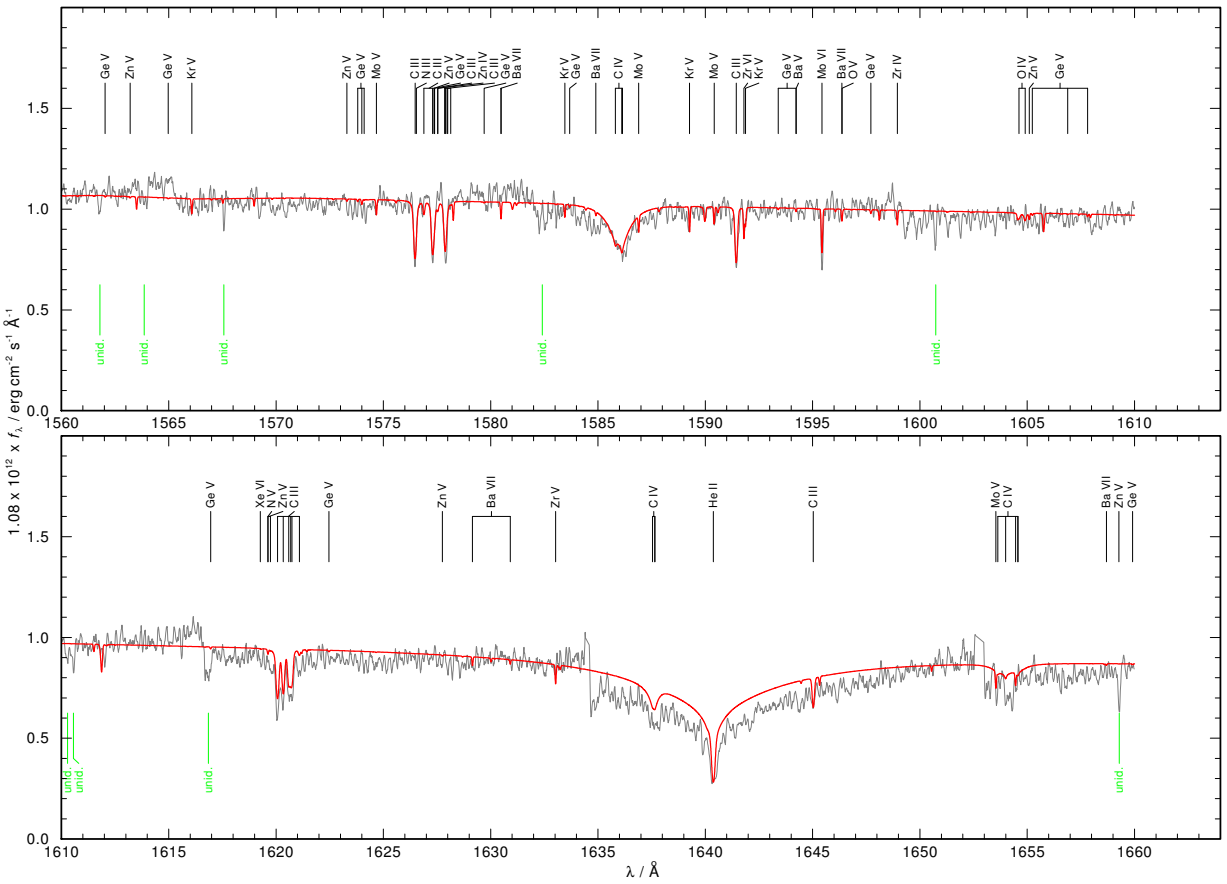

Fig. B.2. continued.

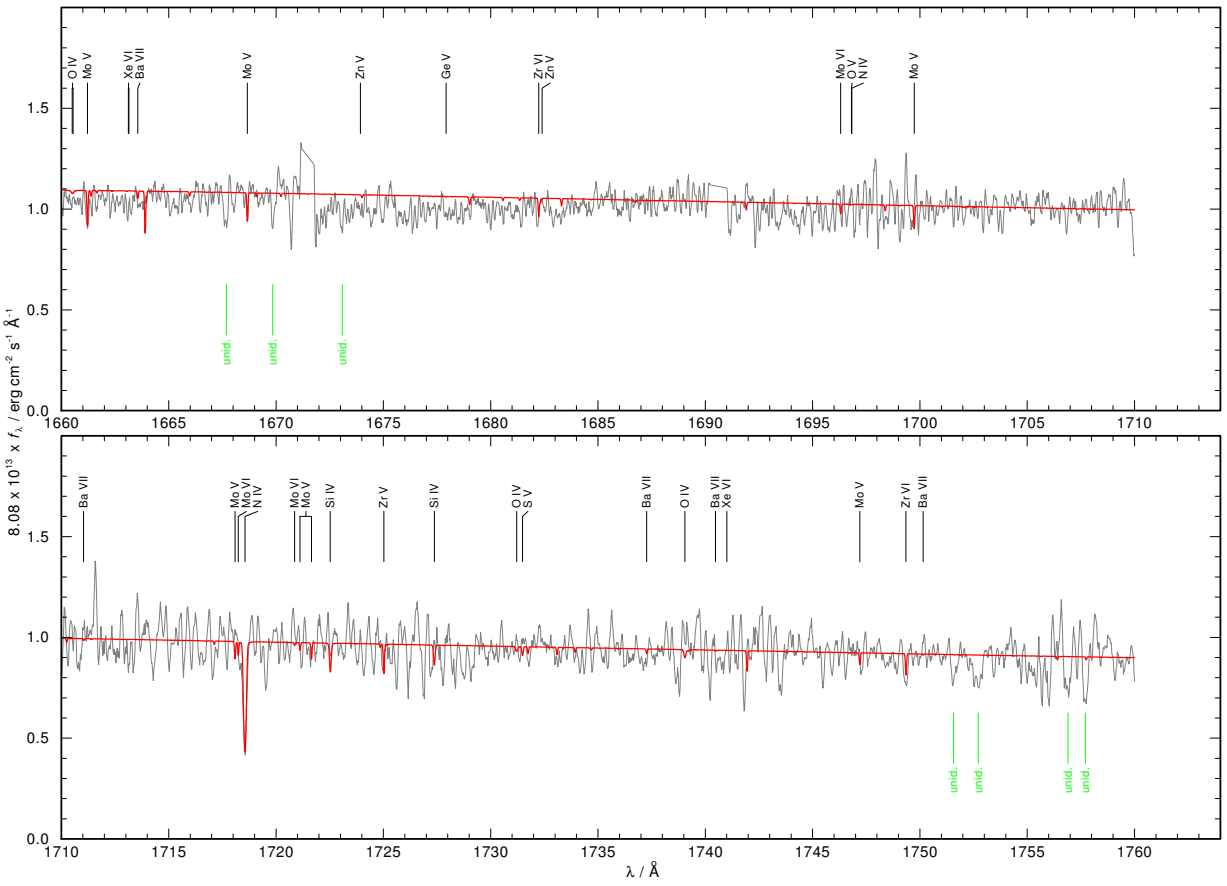

Fig. B.2. continued.

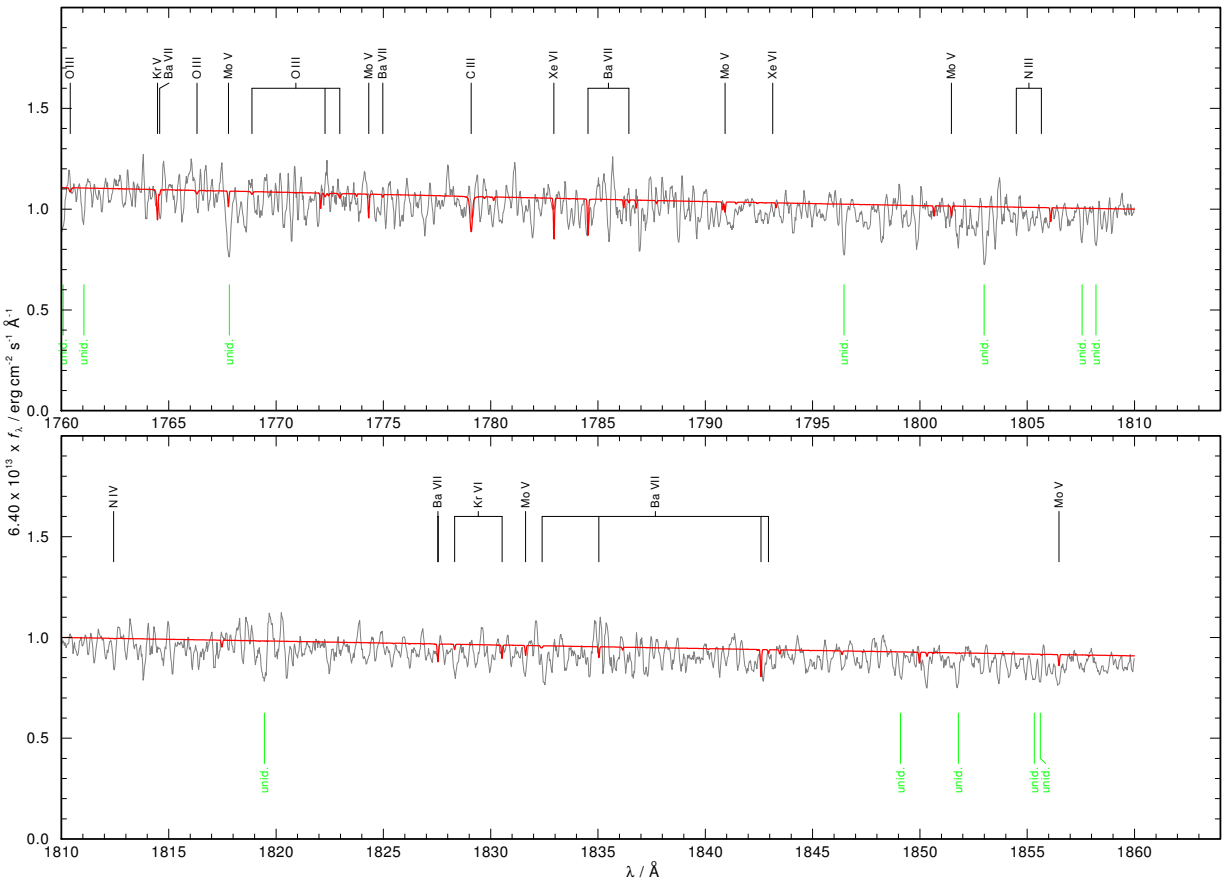

Fig. B.2. continued.

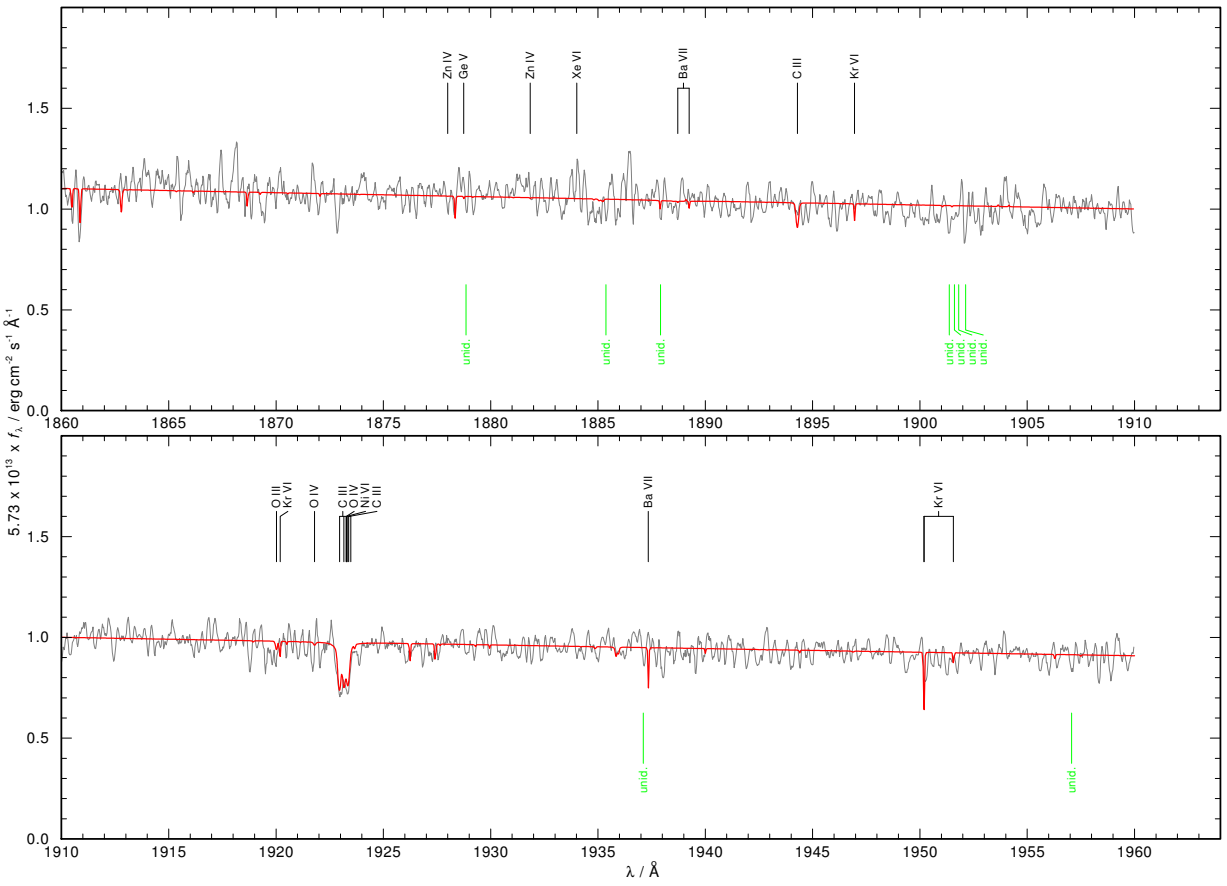

Fig. B.2. continued.

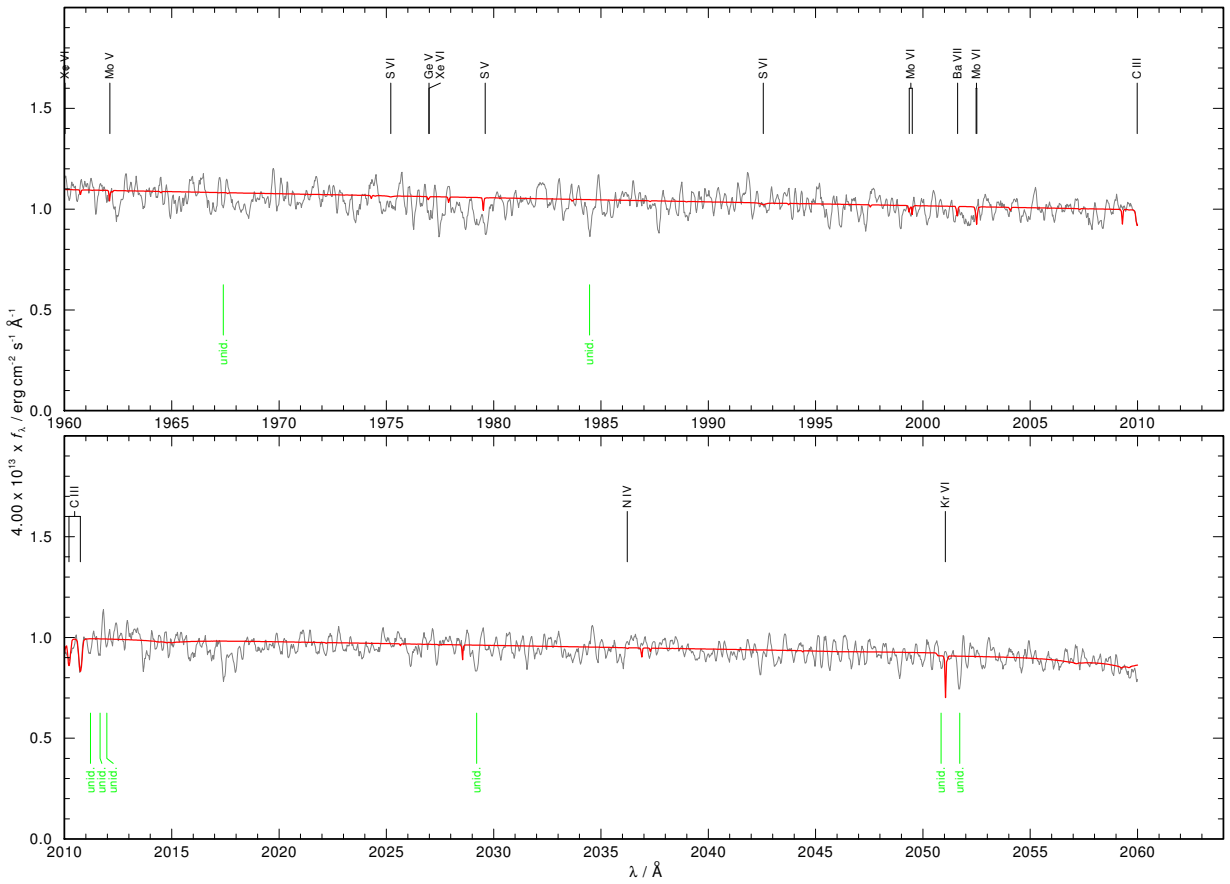

Fig. B.2. continued.

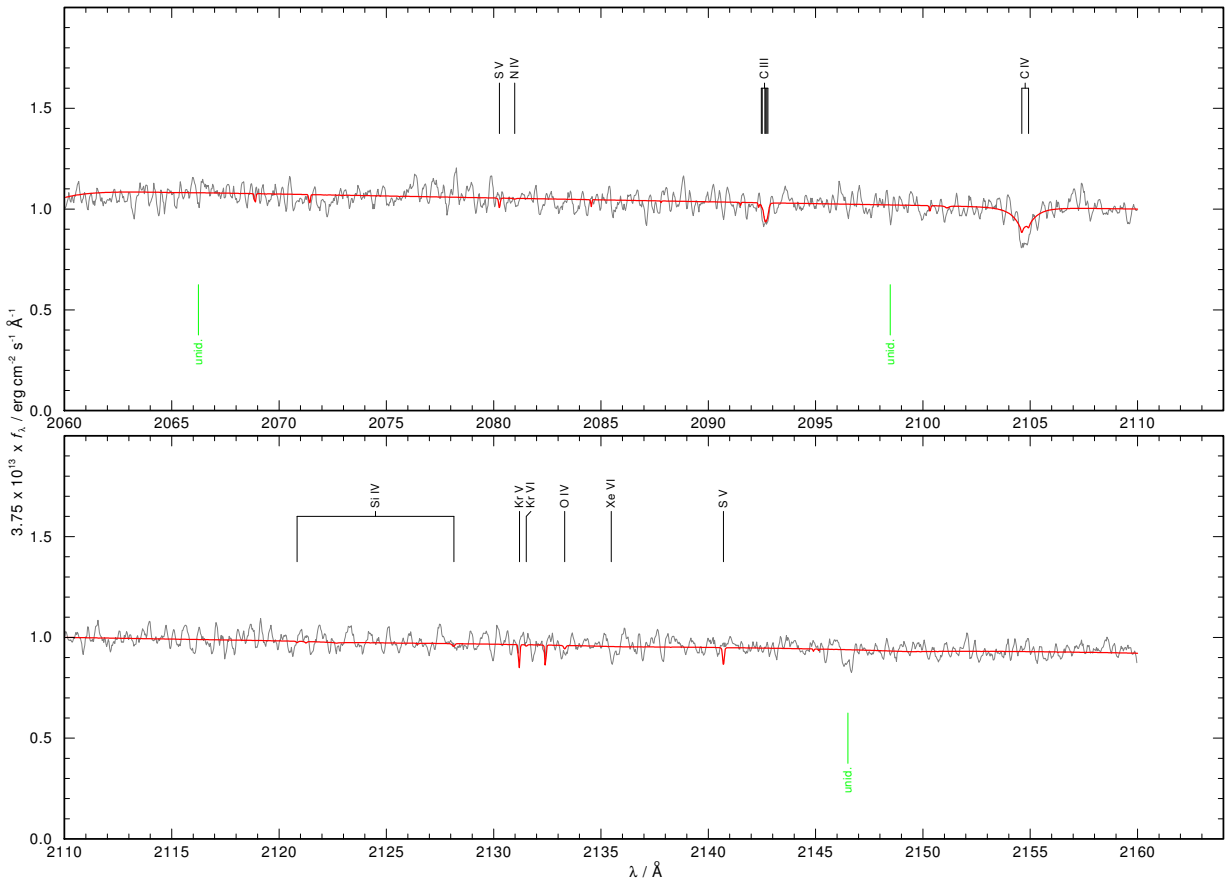

Fig. B.2. continued.

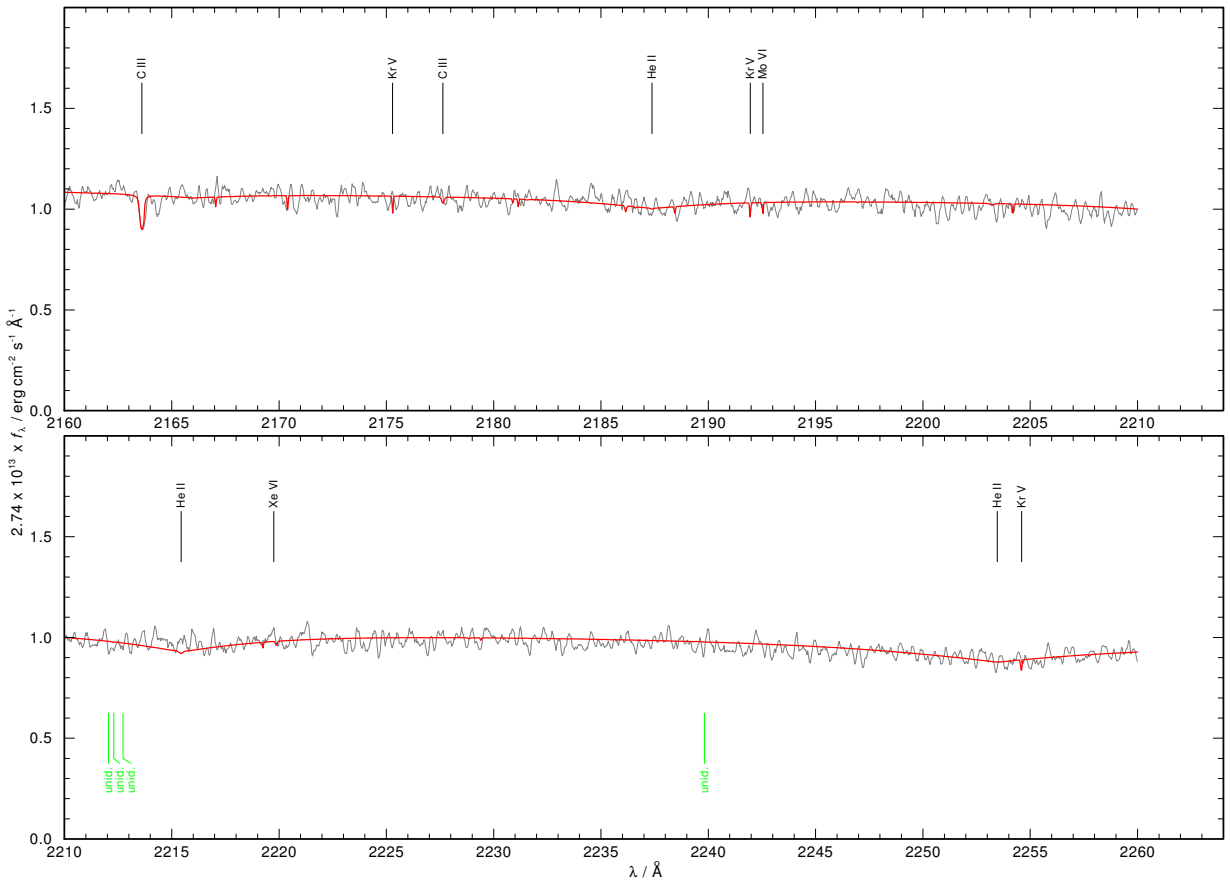

Fig. B.2. continued.

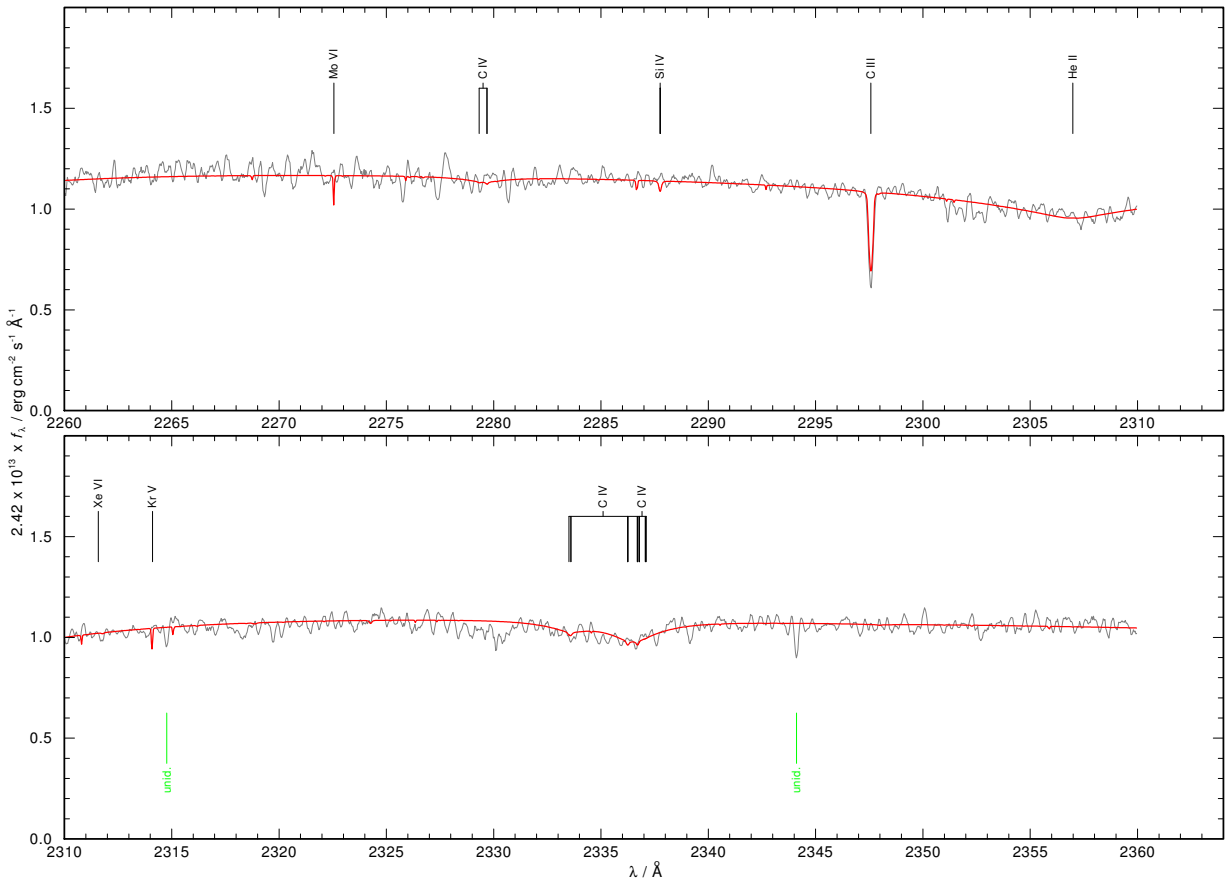

Fig. B.2. continued.

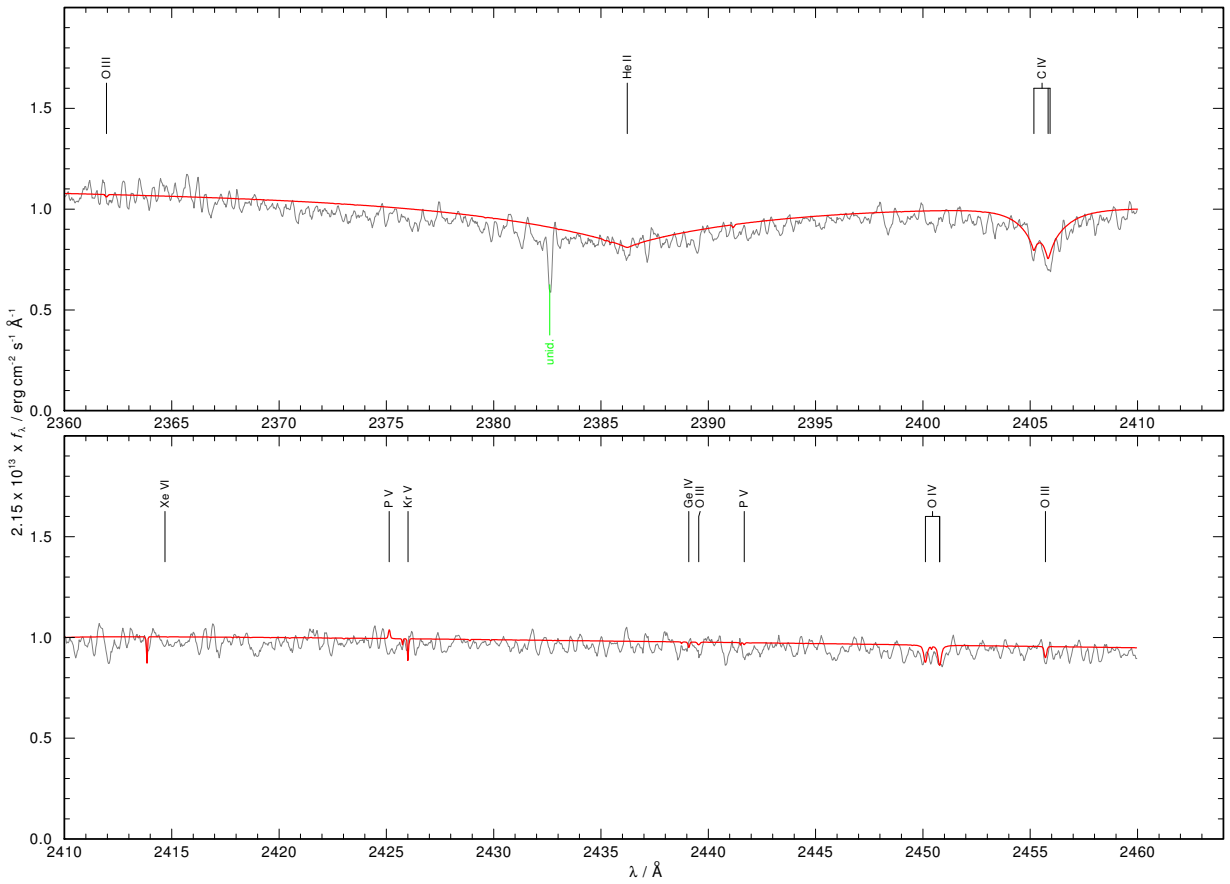

Fig. B.2. continued.

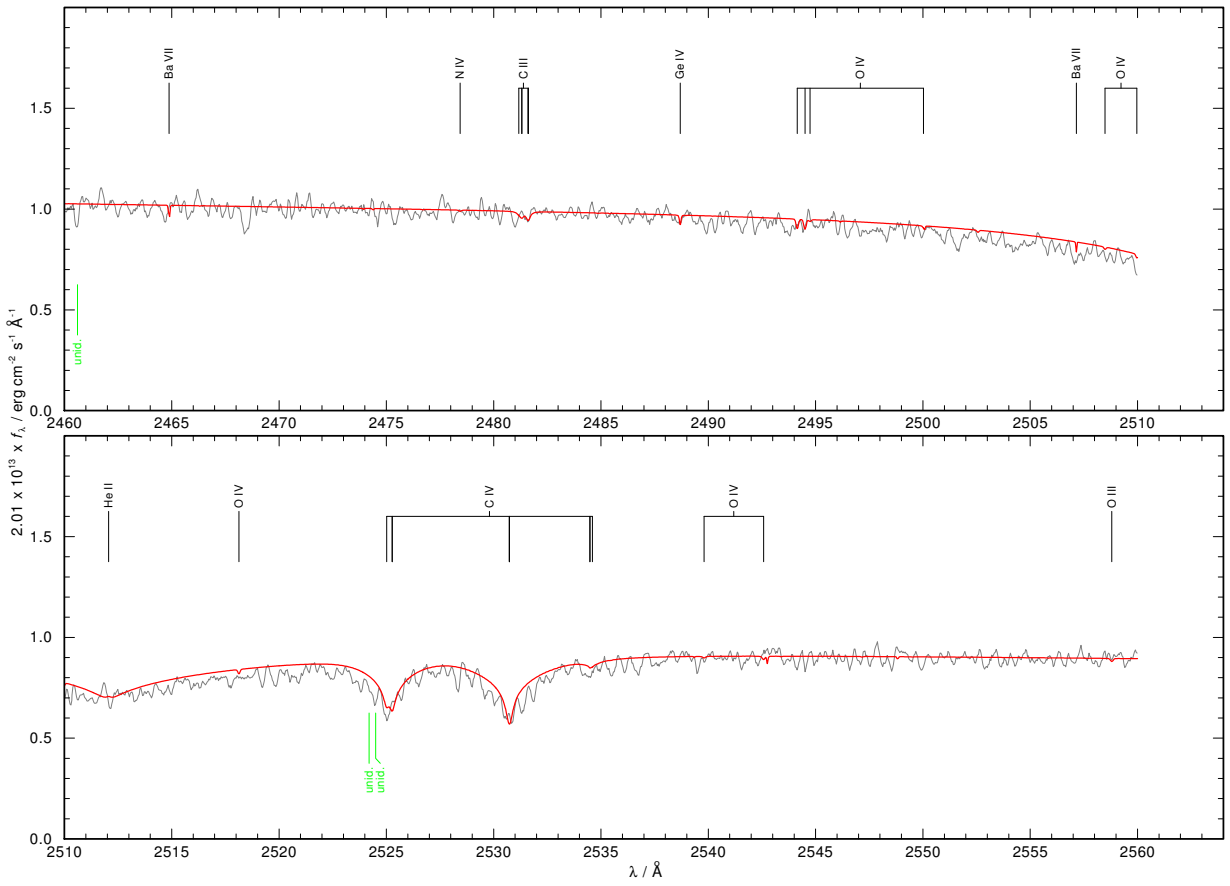

Fig. B.2. continued.

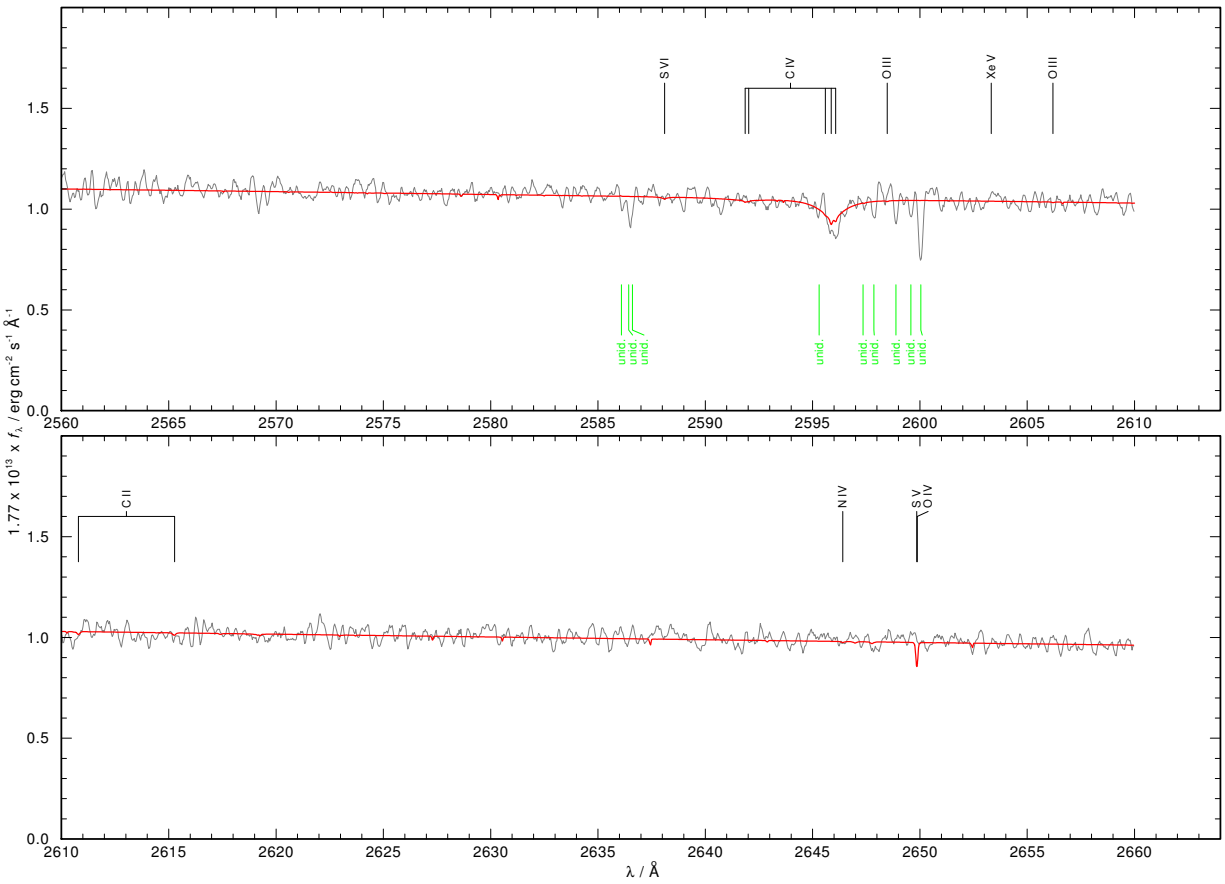

Fig. B.2. continued.

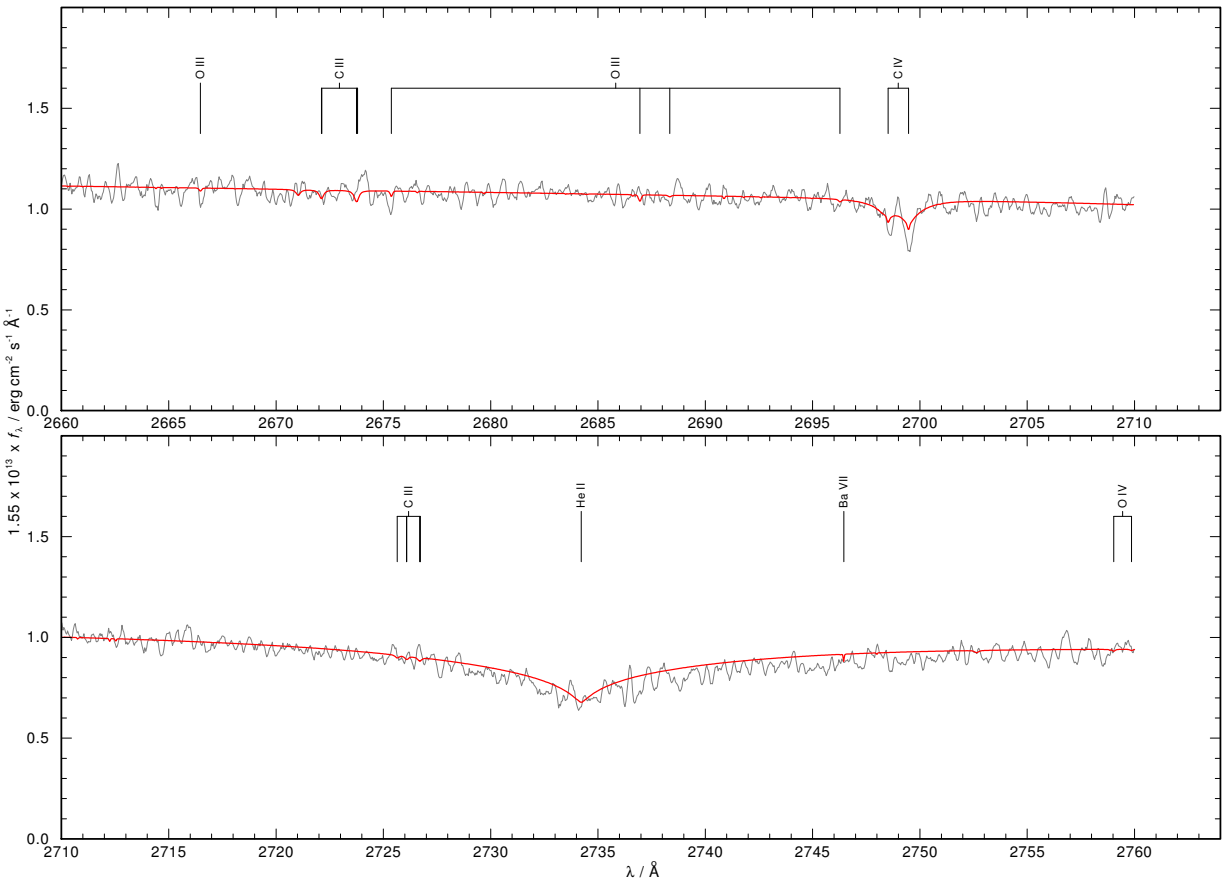

Fig. B.2. continued.

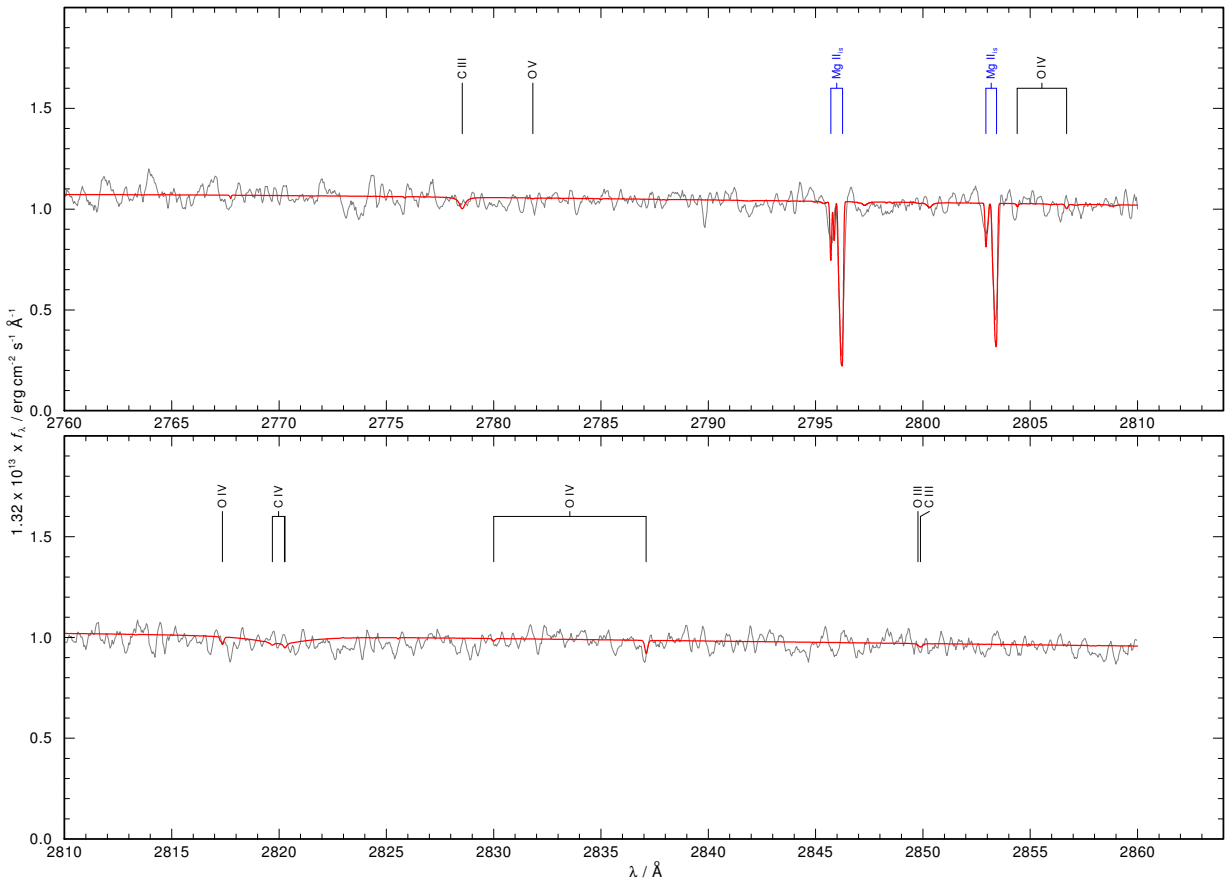

Fig. B.2. continued.

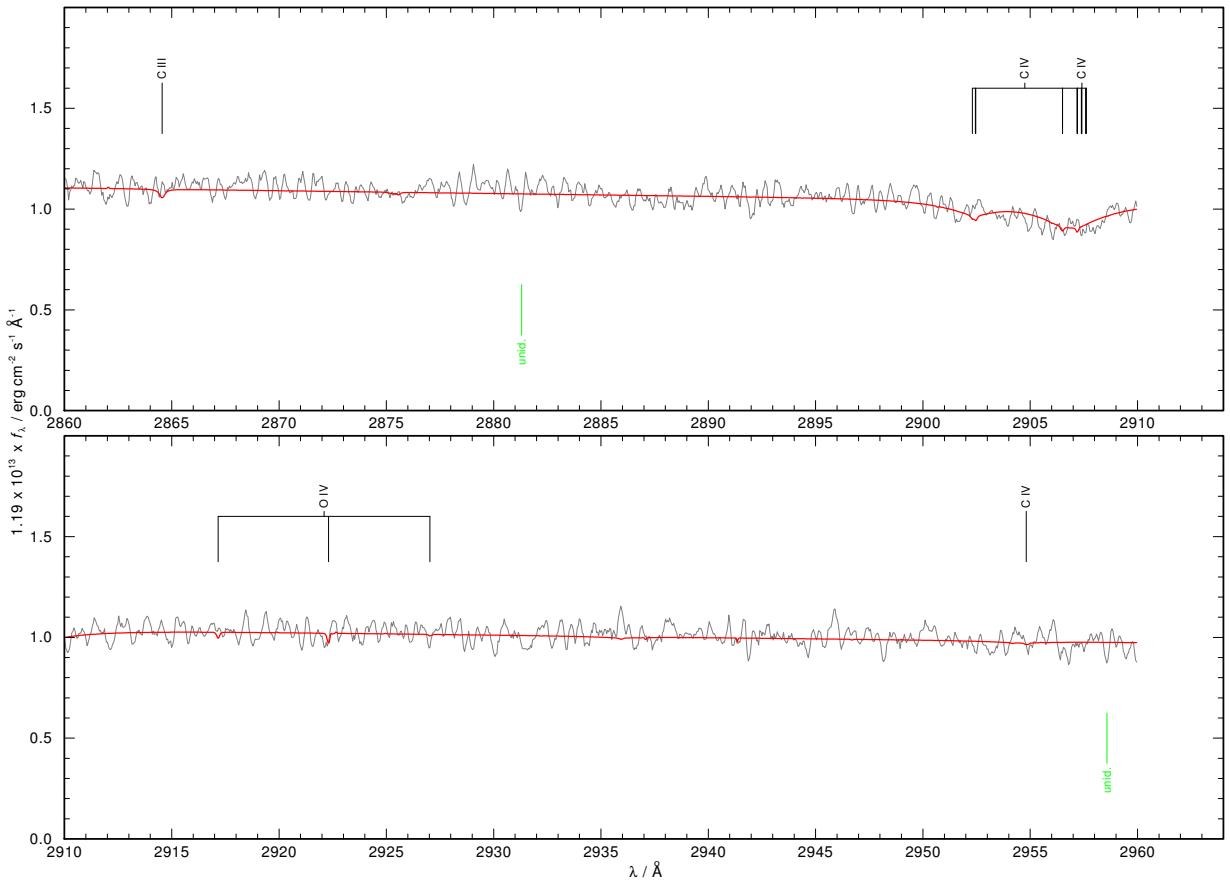

Fig. B.2. continued.

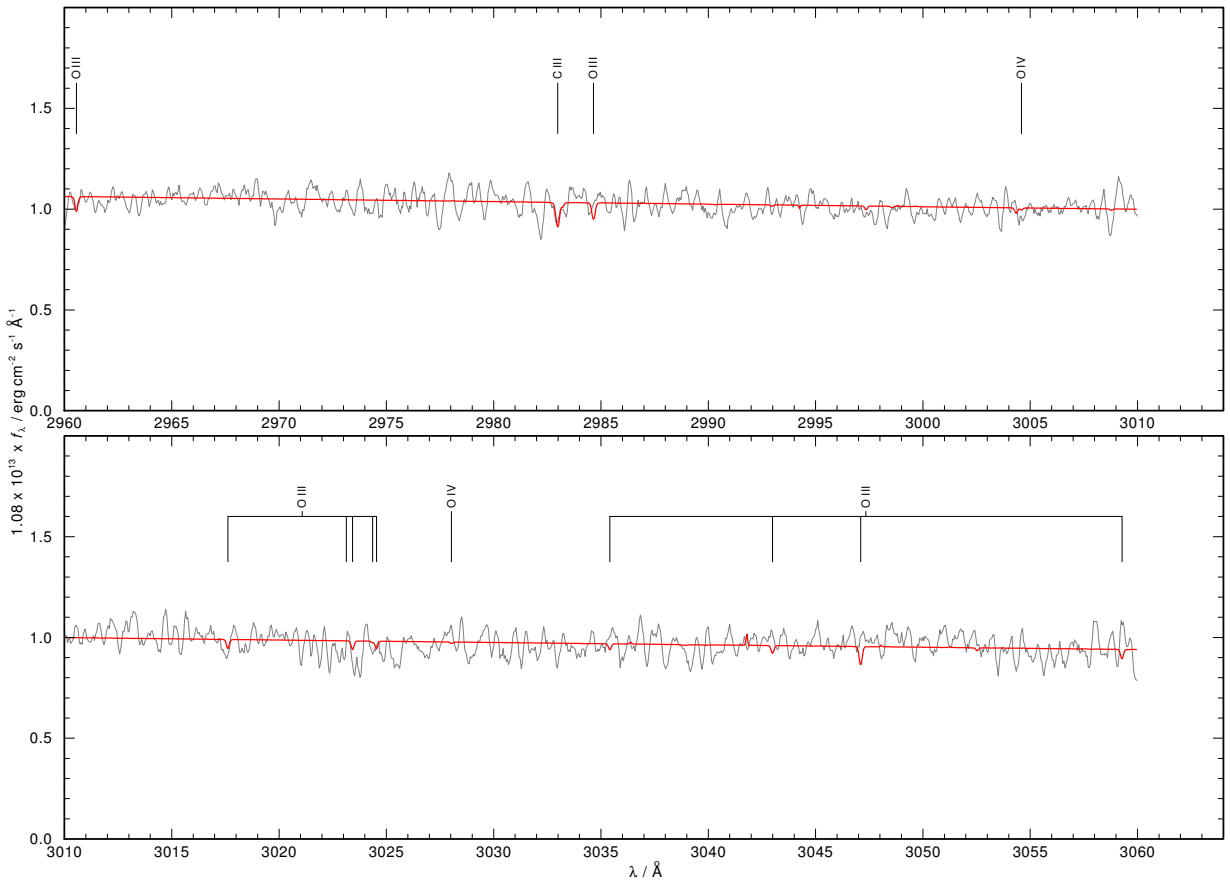

Fig. B.2. continued.

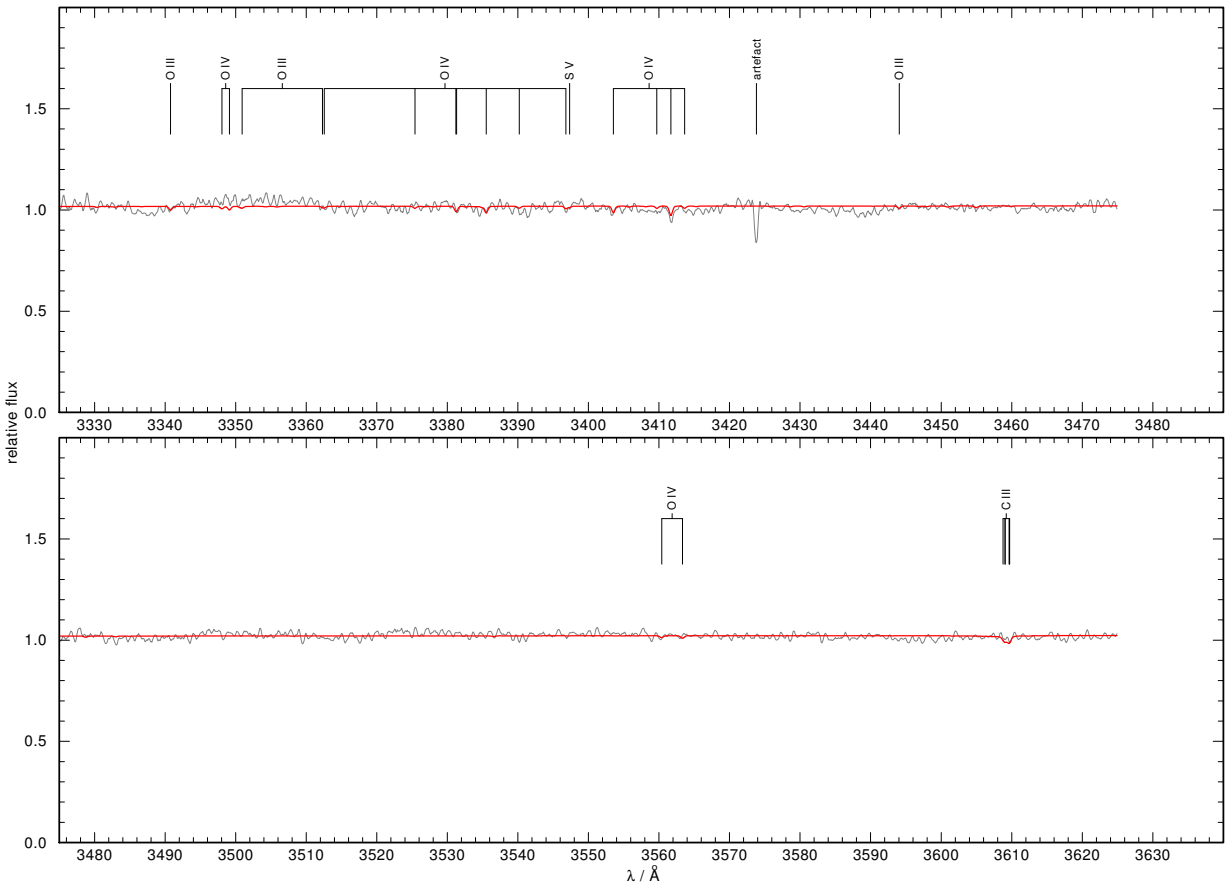

Fig. B.3. Optical (SPY) observation (gray) compared with the best model (red). Stellar lines are identified at top. "unid." denotes unidentified lines.

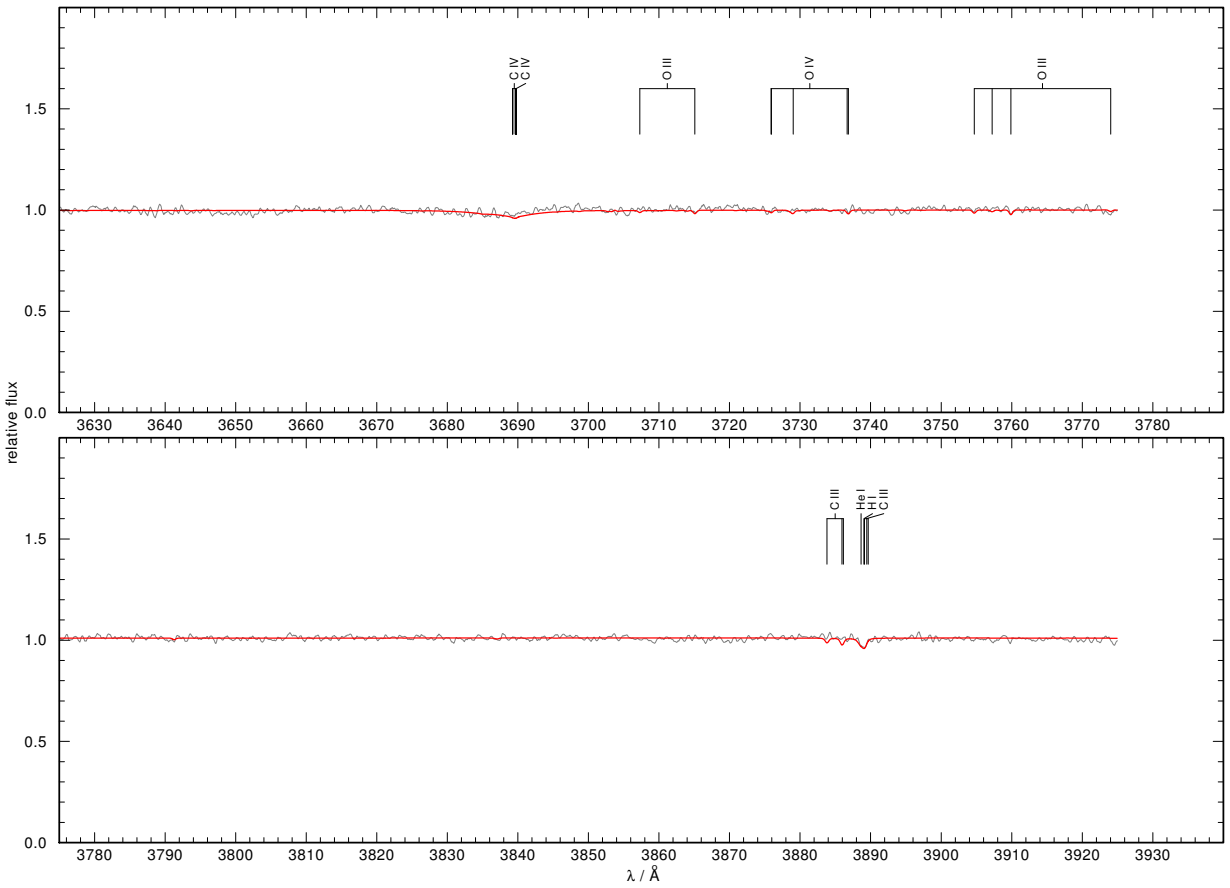

Fig. B.3. continued.

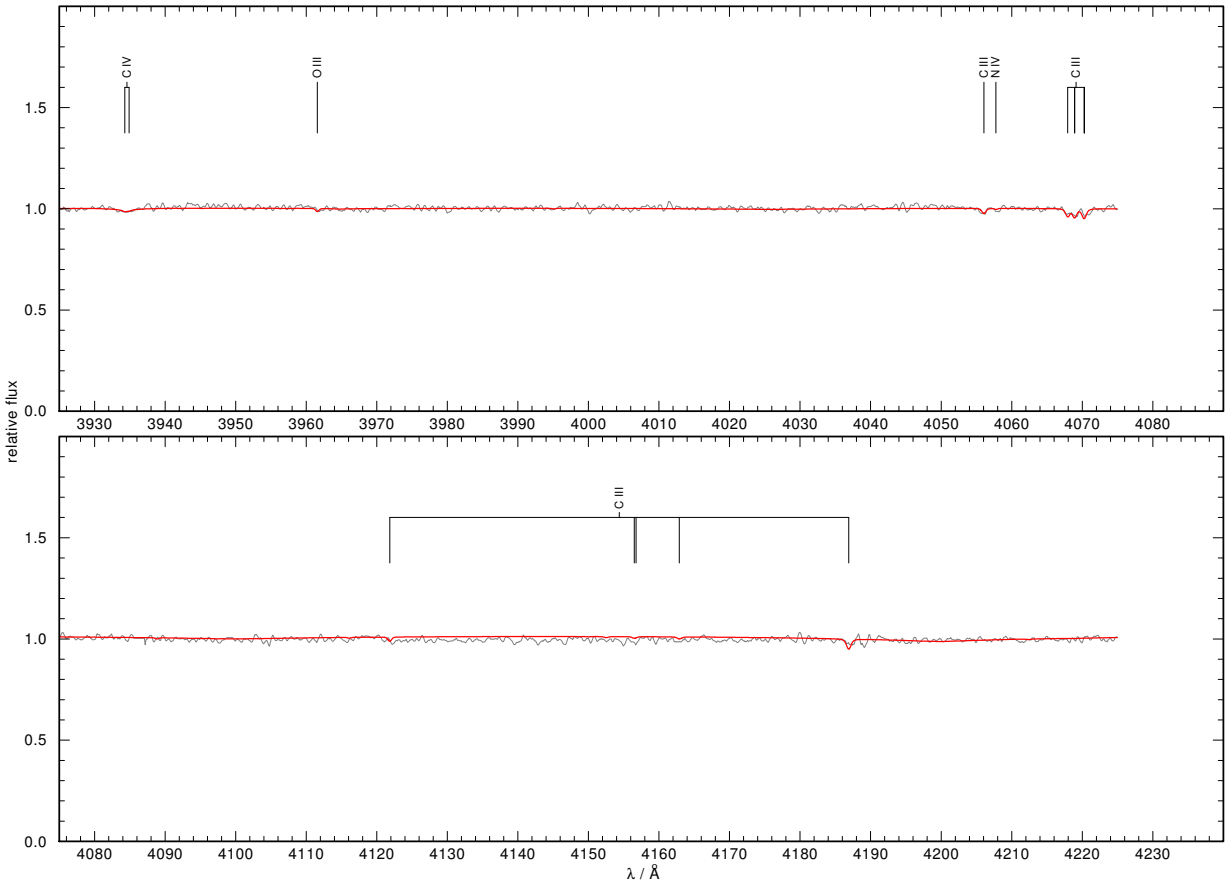

Fig. B.3. continued.

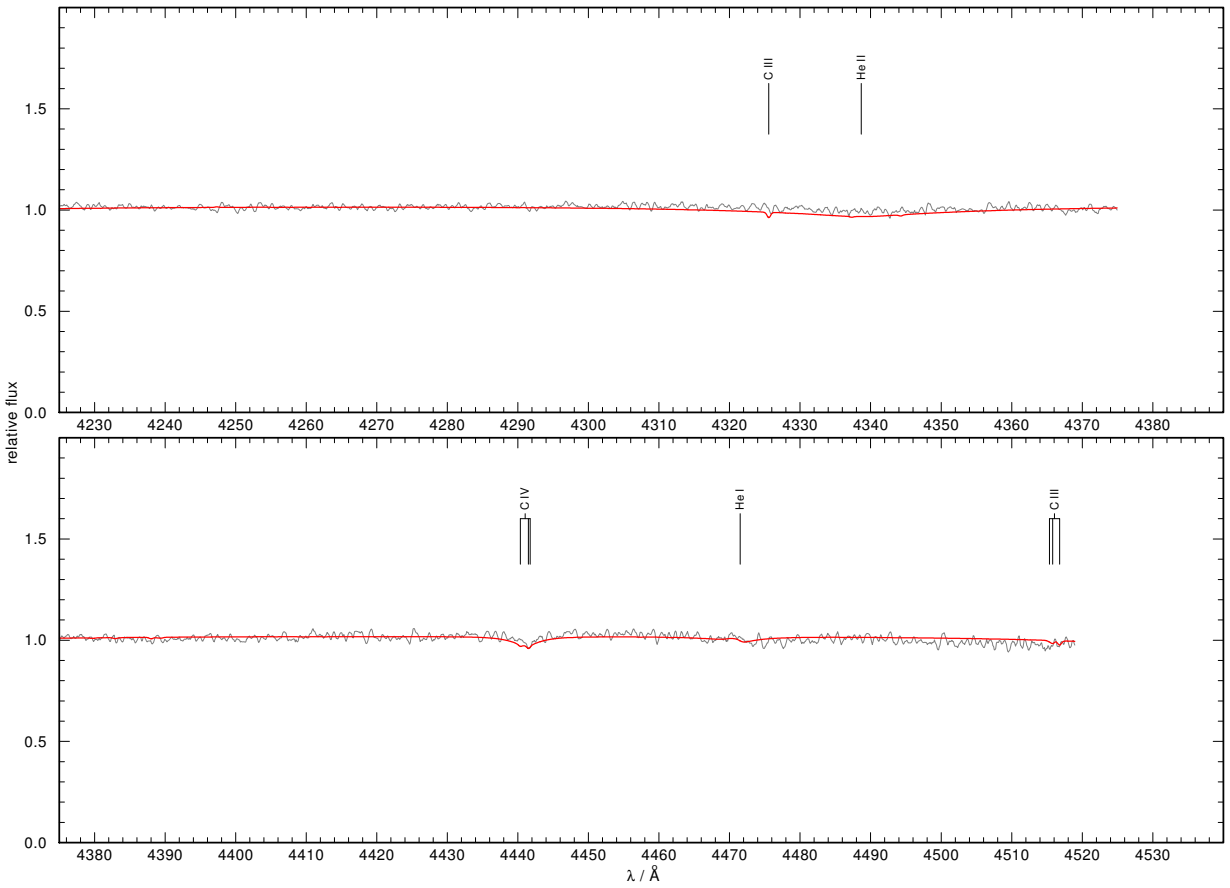

Fig. B.3. continued.

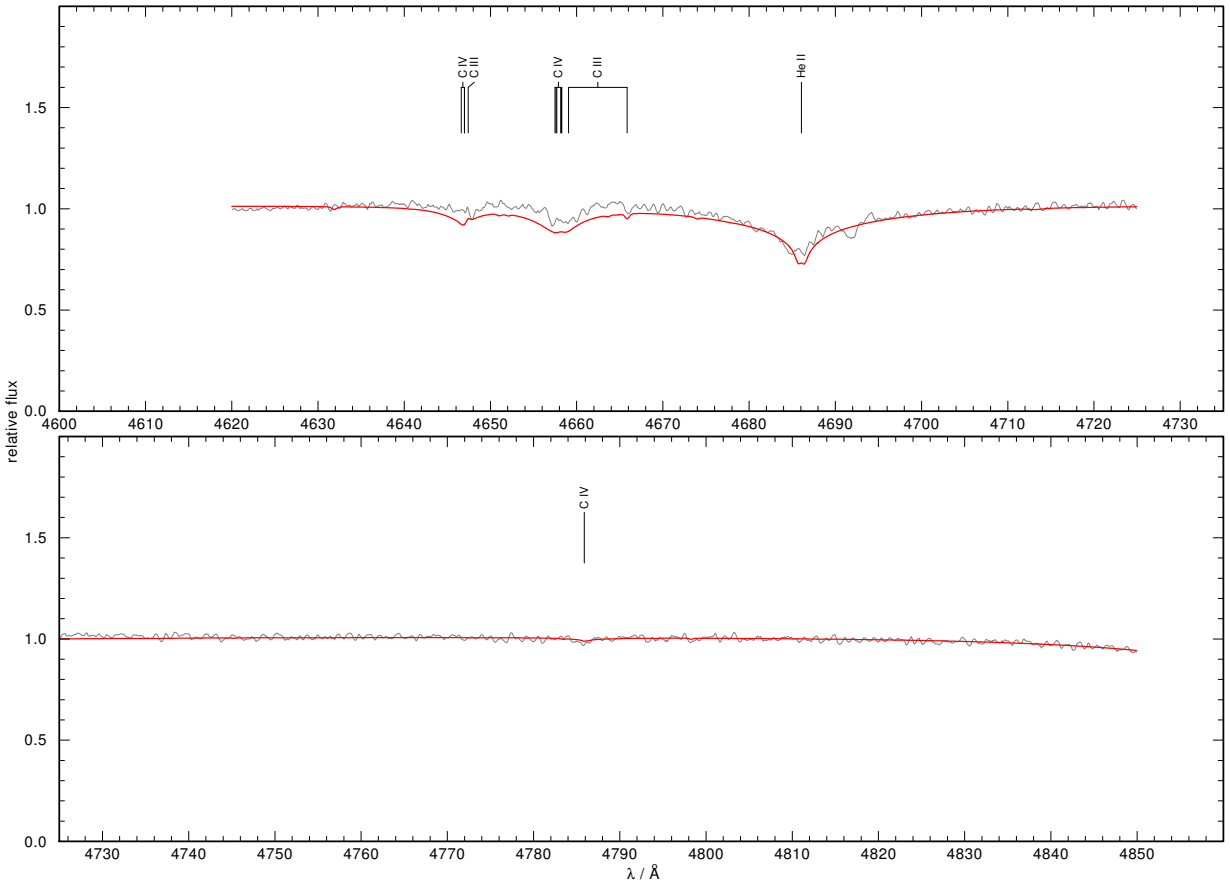

Fig. B.3. continued.

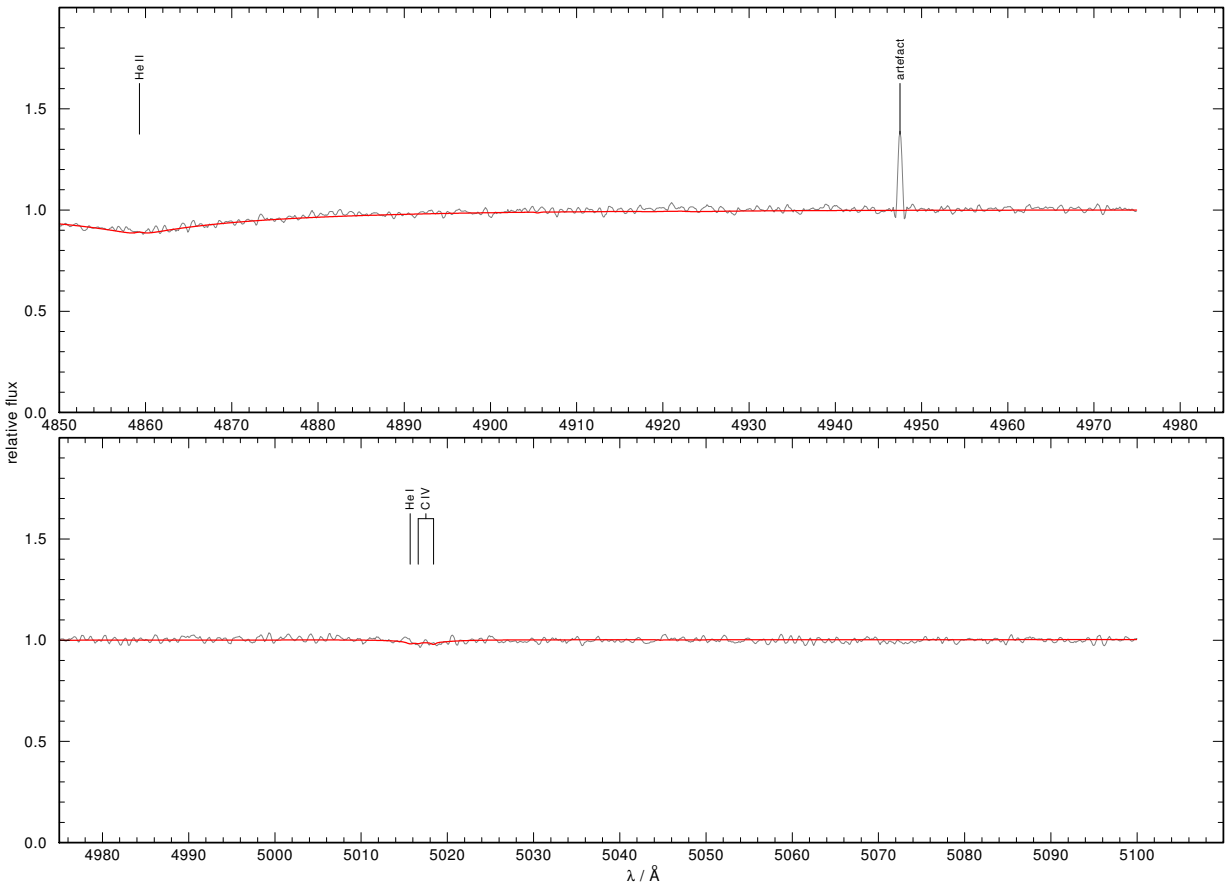

Fig. B.3. continued.

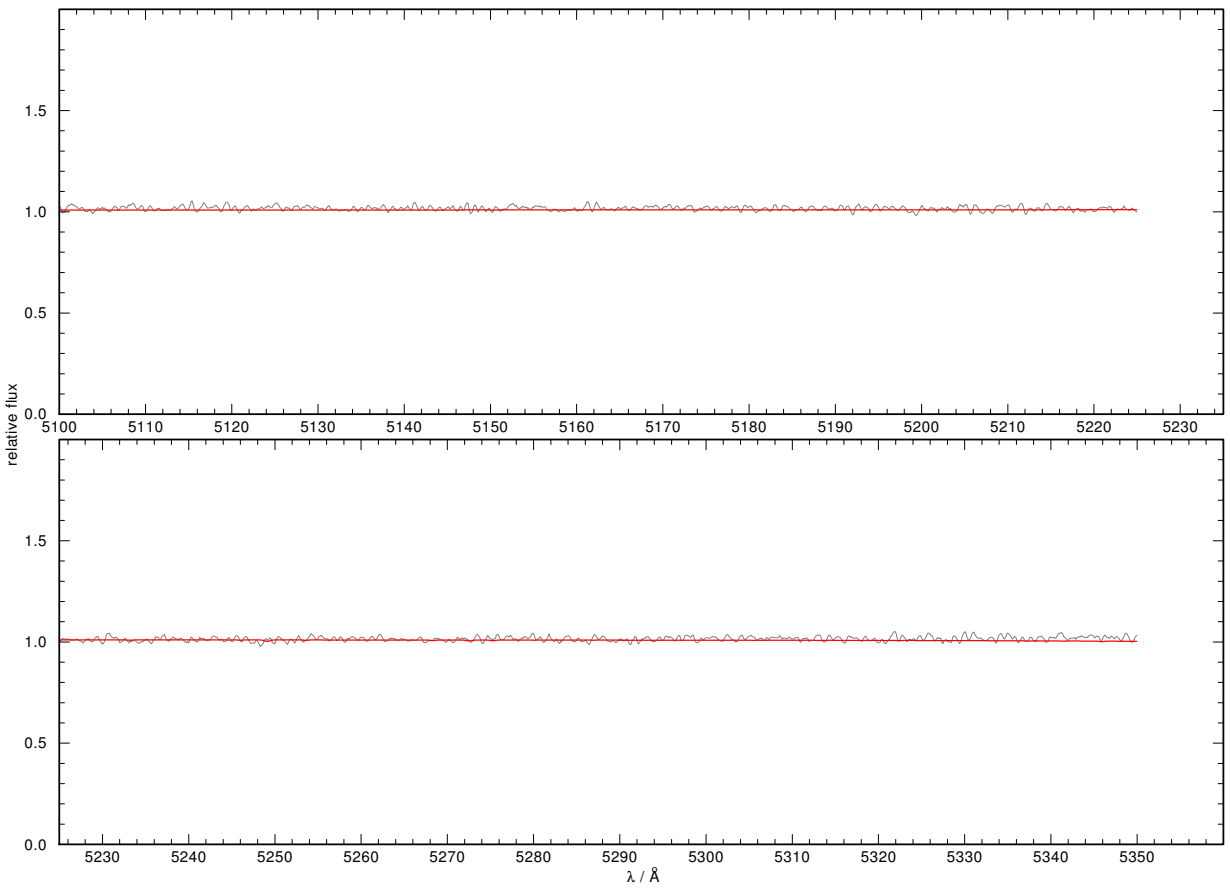

Fig. B.3. continued.

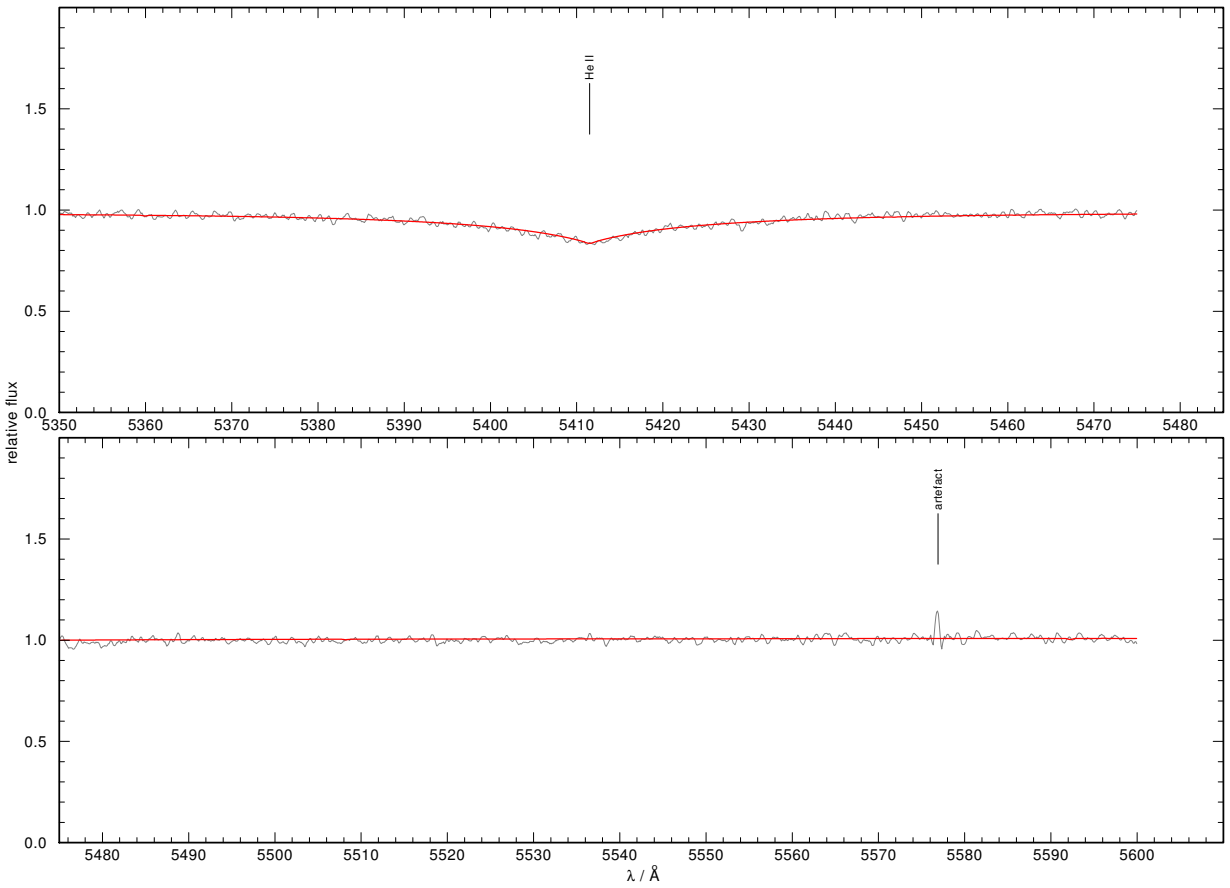

Fig. B.3. continued.

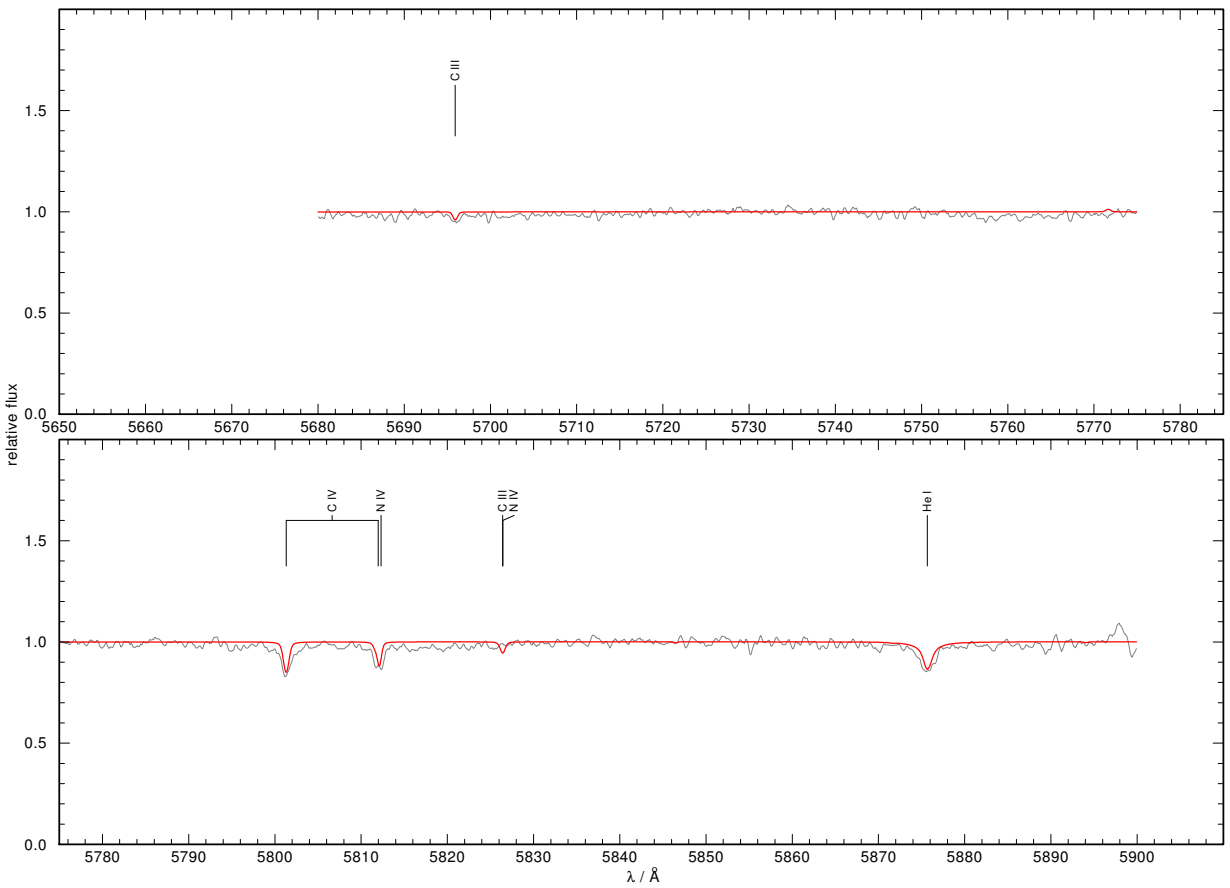

Fig. B.3. continued.

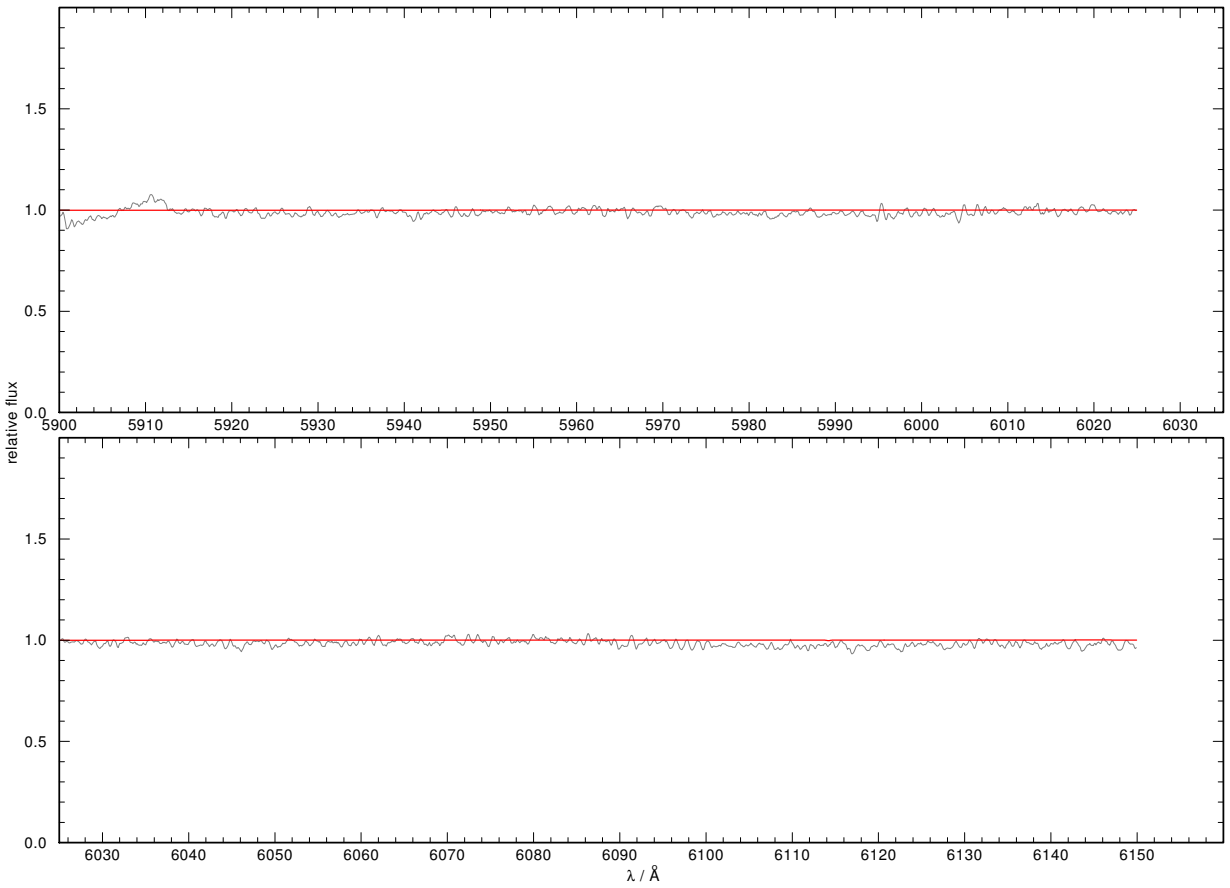

Fig. B.3. continued.

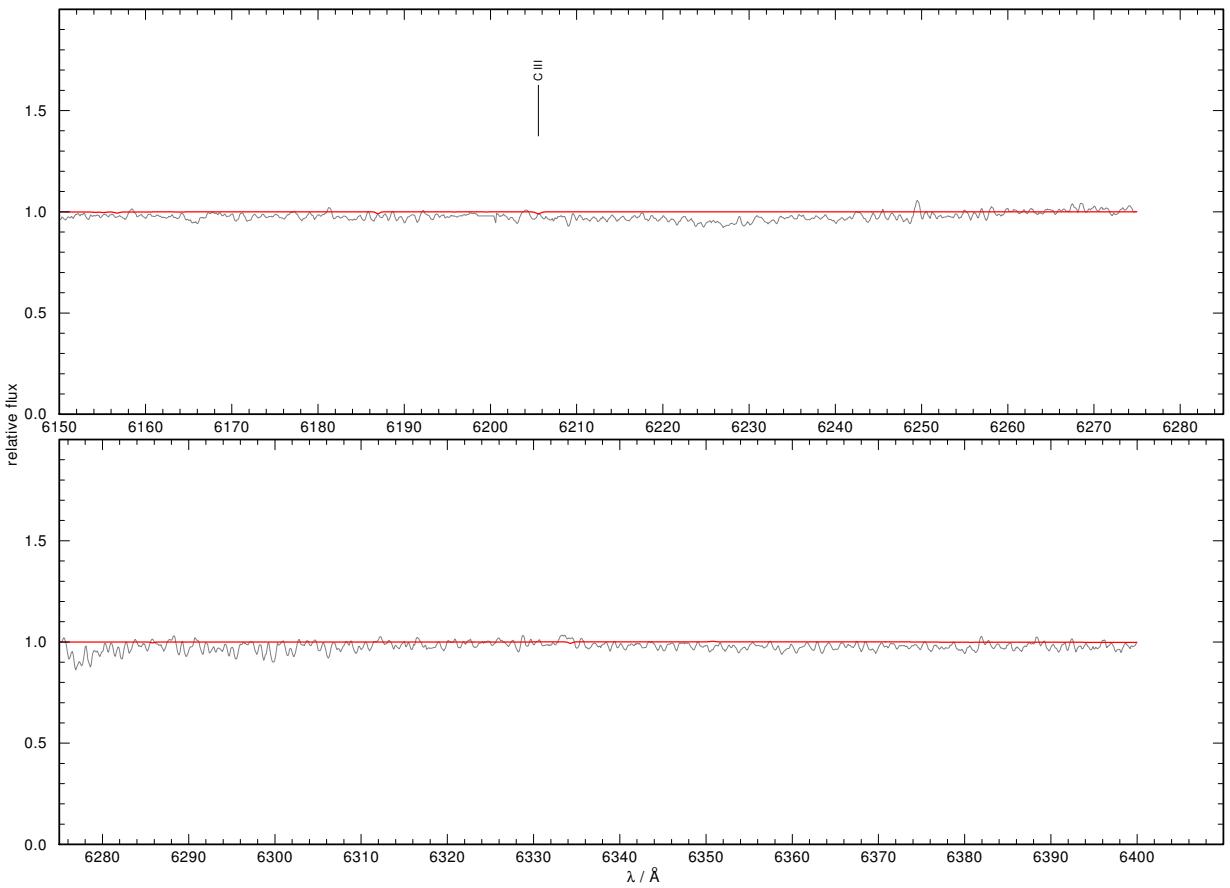

Fig. B.3. continued.

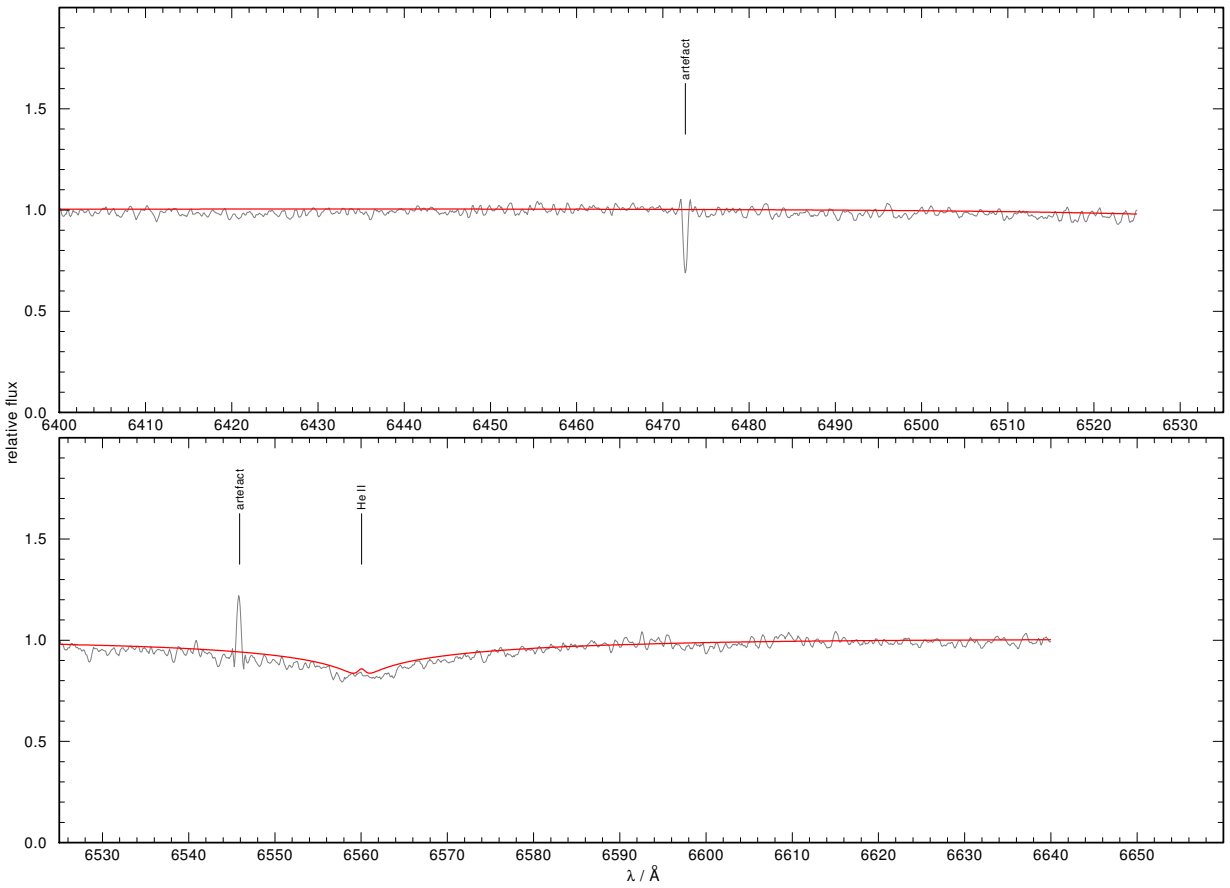

Fig. B.3. continued.

Appendix C: WWW interfaces of TEUV, TGRED, and TVIS

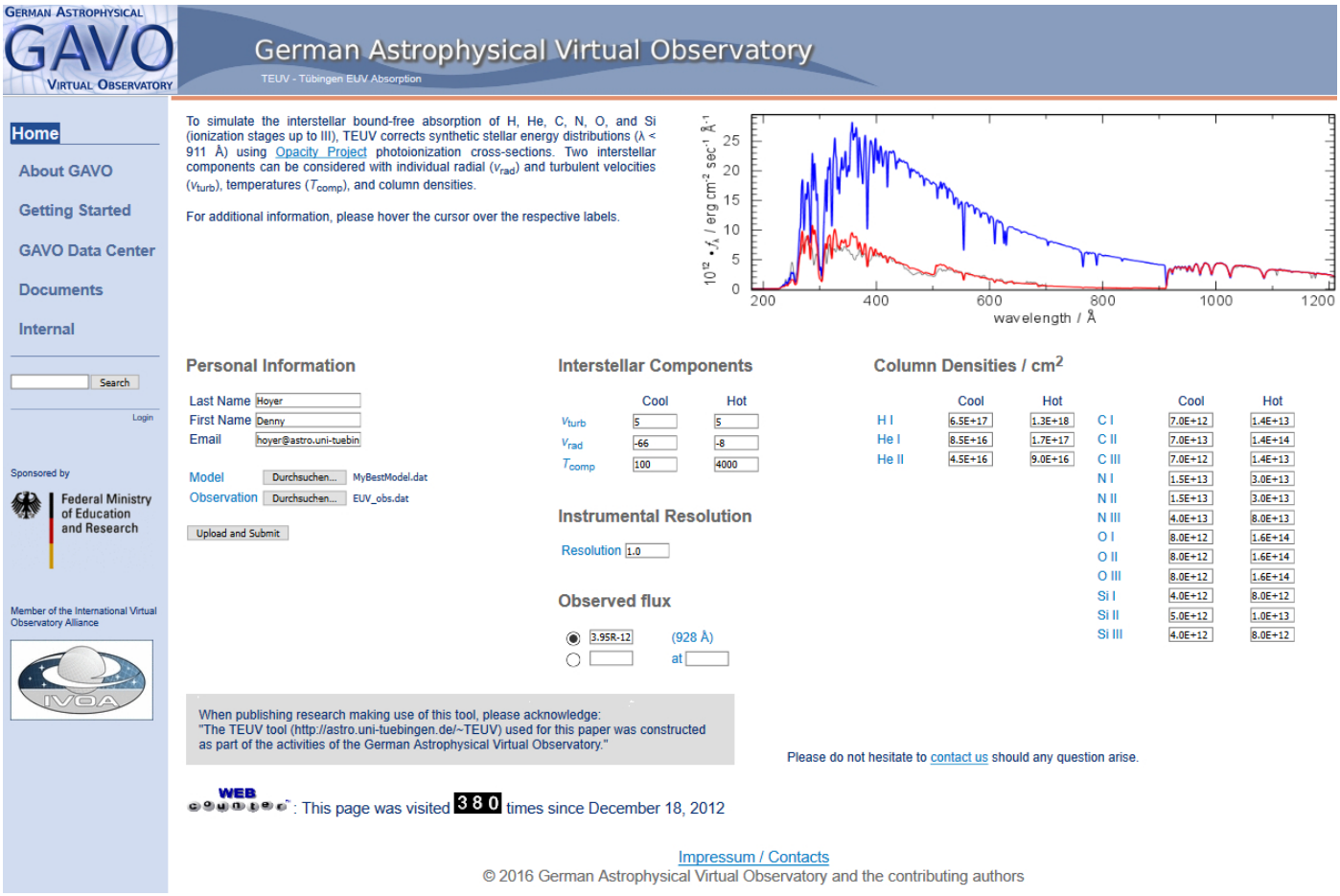

Fig. C.1. TEUV WWW interface.

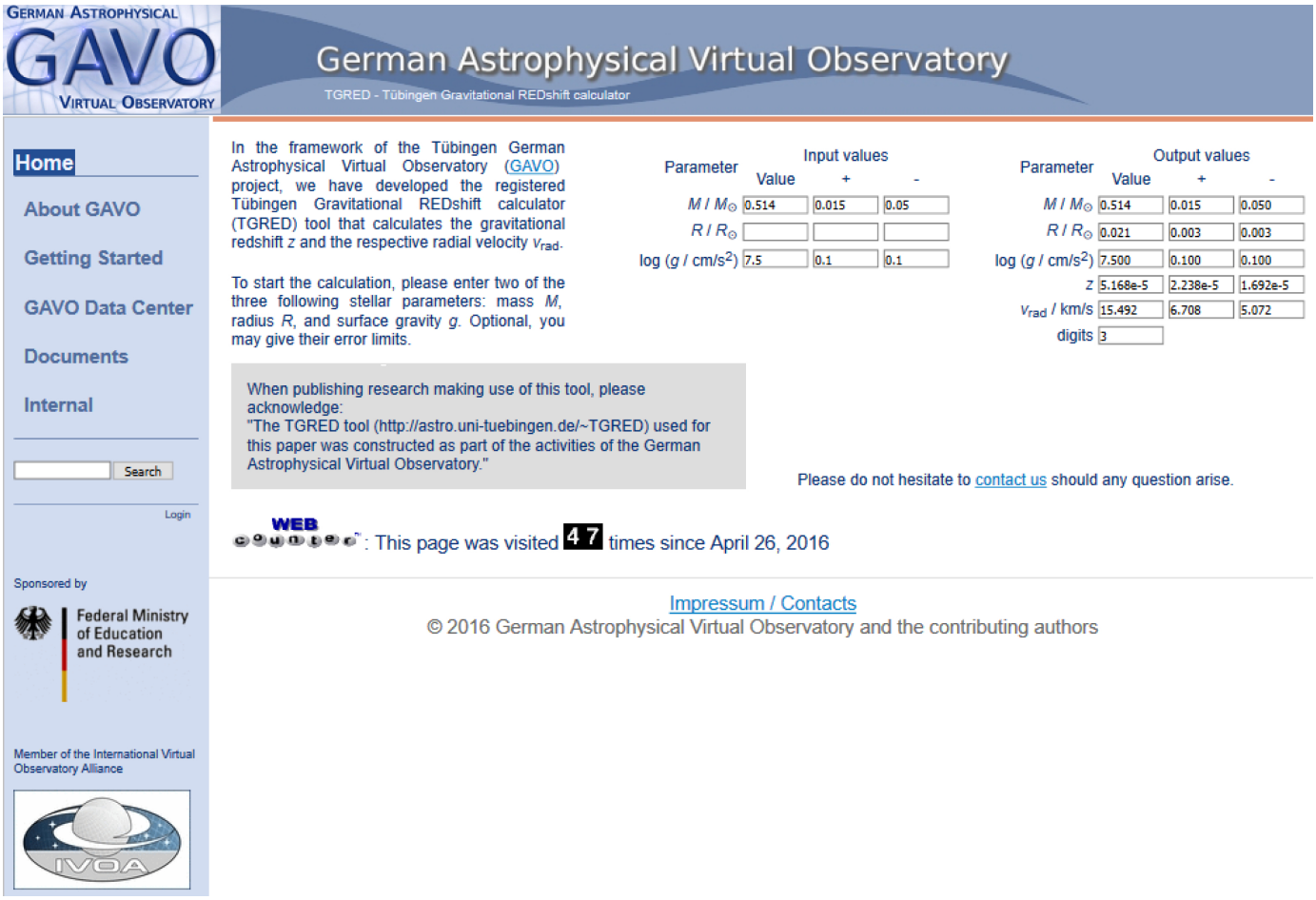

Fig. C.2. TGRED WWW interface.

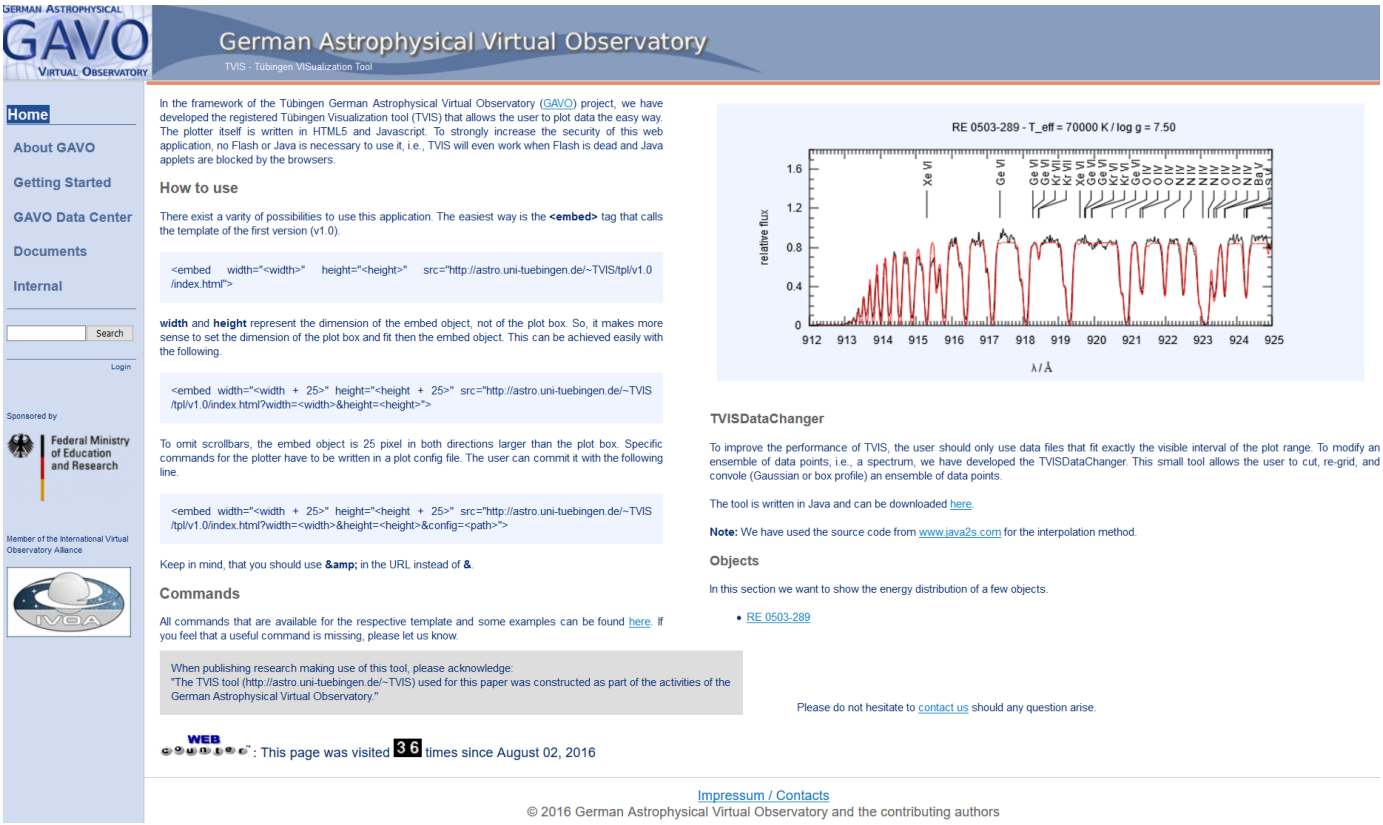

Fig. C.3. TVIS WWW interface.